Ore Geology Reviews 90 (2017) 352–370

Contents lists available at ScienceDirect

Ore Geology Reviews

journal homepage: www.elsevier.com/locate/oregeo

# A laser ablation inductively coupled plasma mass spectrometry study of the distribution of chalcophile elements among sulfide phases in sedimentary and magmatic rocks of the Duluth Complex, Minnesota, USA

N. Samalens *, S.-J. Barnes, E.W. Sawyer

*Sciencesde la Terre, Université du Québec à Chicoutimi, 555 boulevard de l'université, Saguenay, QC G7H 2B1, Canada*

ARTICLE INFO

*Article history:*
Received 5 December 2016
Received in revised form 27 May 2017
Accepted 6 June 2017
Available online 11 June 2017

*Keywords:*
LA-ICP-MS
Black shales
TABS
Ni-Cu sulfide deposits
Duluth Complex

ABSTRACT

Nickel-copper sulfide deposits occur in the basal unit of the Partridge River Intrusion, Duluth Complex (Minnesota, USA). Many lines of evidence suggest that these sulfides are formed after assimilation of the proterozoic S-rich black shales, known as the Bedded Pyrrhotite Unit. In addition to S, black shales are enriched in Te, As, Bi, Sb and Sn (TABS) and the basaltic magma of the intrusion is contaminated by the partial melt of the black shales. The TABS are chalcophile and together with the platinum-group elements, Ni and Cu partitioned into the magmatic sulfide liquid that segregated from the Duluth magma. The TABS are important for the formation of platinum-group minerals (PGM) thus their role during crystallization of the base metal sulfide minerals could affect the distribution of the PGE. However, the concentrations of TABS in magmatic Ni-Cu-PGE deposits and their distribution among base metal sulfide minerals are poorly documented. In order to investigate whether the base metal sulfide minerals host TABS in magmatic Ni-Cu-PGE deposits, a petrographic and Laser Ablation Inductively Coupled Plasma Mass Spectrometry (LA-ICP-MS) study has been carried out on base metal sulfide and silicate phases of the Partridge River Intrusion, Duluth Complex.

Petrographic observations showed that the proportions of the base metal sulfide minerals vary with rock type. The sulfide assemblage of the least metamorphosed Bedded Pyrrhotite Unit from outside the contact metamorphic aureole consists of pyrite with minor pyrrhotite plus chalcopyrite (<5%), whereas within the contact aureole the sulfide assemblage of the Bedded Pyrrhotite Unit rocks consists dominantly of pyrrhotite (>95%) with small amount of chalcopyrite (<2%). The sulfide mineral assemblage in the xenoliths of the Bedded Pyrrhotite Unit and in the mafic rocks of the basal unit contains two additional sulfides, pentlandite and cubanite.

Our LA-ICP-MS study shows that sulfides of the Bedded Pyrrhotite Unit are rich in TABS; consistent with these S-rich black shales being the source of TABS that contaminated the mafic magma. Most of the TABS are associated with sulfides and platinum-group minerals in the rocks of the Bedded Pyrrhotite Unit from the contact aureole, the Bedded Pyrrhotite Unit xenoliths and the mafic rocks of the Duluth Complex. In addition to these phases the laser maps show that silicate phases, i.e., orthopyroxene and plagioclase contain Sn and Pb respectively. In contrast, in the least metamorphosed samples of the Bedded Pyrrhotite Unit from outside the contact aureole although the pyrite contains some TABS mass balance calculations indicates that most the TABS are contained in other phases. In these rocks, galena hosts significant amounts of Te, Bi, Sb, Sn and Ag and few very small grains of Sb-rich phases were also observed. The host phases for As were not established but possibly organic compounds may have contributed.



## 1. Introduction

Most of world's Ni-Cu-Platinum-group element (PGE) deposits are thought to have formed after contamination of a mafic magma with S-bearing sedimentary rocks (Lesher and Burnham, 2001;

* Corresponding author.
*E-mail address:* n.samalens@gmail.com (N. Samalens).

http://dx.doi.org/10.1016/j.oregeorev.2017.06.007
0169-1368/

Ripley and Li, 2013). In particular, S-rich black shales are an ideal potential source of S (Lesher and Burnham, 2001; Robertson et al., 2015).

In addition to S, black shales are enriched in most chalcophile elements, including a group of elements Te, As, Bi, Sb and Sn (hereafter these elements will be referred to as TABS, see also Barnes and Ripley, 2016) important in the formation of platinum-group minerals. However, in contrast to PGE, the concentration of TABS and their host minerals are poorly documented in Ni-Cu-PGE sulfide deposits (Barnes and Ripley, 2016).

The Duluth Complex is an ideal place to study the distribution of chalcophile elements between phases in a Ni-Cu-PGE sulfide deposit. At the Duluth Complex S-rich black shales of the Bedded Pyrrhotite Unit (~0.5 to 10% S) in the Virginia Formation are found both at the contact with the intrusion and as xenoliths in the basal unit of the Partridge River Intrusion (Mainwaring and Naldrett, 1977; Ripley, 1981; Andrews and Ripley, 1989; Thériault et al., 1997; Thériault and Barnes, 1998; Ripley et al., 2007; Severson and Hauck, 2008; Queffurus and Barnes, 2014). This basal unit also contains Ni-Cu-PGE deposits in the form of disseminated and less commonly massive sulfides. Numerous drill holes across the basal unit and into the country rocks allow detailed sampling.

The Bedded Pyrrhotite Unit contains similar concentrations of TABS, i.e., As 38 ppm, Sb 4.1 ppm and Bi 0.6 ppm and Te 0.4 ppm, to black shales from the literature and is considerably enriched in these elements when compared to basaltic magmas and the average of upper crust (Samalens et al., 2017; Table 1). The Bedded Pyrrhotite Unit has been identified as the source of the sulfur (Zanko et al., 1994; Queffurus and Barnes, 2014) and TABS (Samalens et al., 2017) that contaminated the mafic magma at the Duluth Complex.

To investigate the distribution of TABS among phases we have carried out a petrographic study and combined with a laser ablation analyzes and chemical mapping of sedimentary and magmatic sulfides and silicate phases at the Duluth Complex.

## 2. Geological context

The mid-Proterozoic (1100 Ma) Duluth Complex is located in Minnesota, USA. It consists of a number of mafic intrusions (Fig. 1) that were emplaced into the Midcontinent Rift System and are related to the overlying Keweenawan flood basalt (Severson and Hauck, 1997; Ojakangas et al., 2001; Miller and Severson, 2002). Magmatic Ni-Cu deposits occur at the base of two of the intrusions (Fig. 1), the Partridge River (see description below) and the South Kawishiwi (recent studies of Cu-Ni-PGE mineralization in Gál et al., 2013; Benkó et al., 2015a,b; Raic et al., 2015).

Our study focused on the deposits of the Partridge River Intrusion (Fig. 2). The basal unit is composed of the following lithologies: norite, gabbronorite, troctolite and peridotites from the bottom to the top of the unit (Hauck et al., 1997; Thériault et al., 1997; Miller and Severson, 2002; Severson and Hauck, 2008). Thériault et al. (1997) and Queffurus and Barnes (2014) interpreted the norites as corresponding to the contaminated part of the magma as they are located in the vicinity of xenoliths in the basal part of the intrusion. The Ni-Cu-PGE deposits consist mainly of disseminated sulfides. The main minerals present are pyrrhotite, cubanite, chalcopyrite and pentlandite (Thériault and Barnes, 1998; Ripley, 2014). Disseminated sulfides are found throughout the basal unit of the Partridge River Intrusion.

The country rocks of the Partridge River Intrusion are lower Proterozoic sedimentary rocks of the Virginia Formation; part of the Animikie Group (Fig. 2). The Virginia Formation is composed of carbonates, greywackes, pelites, black shales and siltstones (Lucente and Morey, 1983). Away from the intrusion the sedimen-

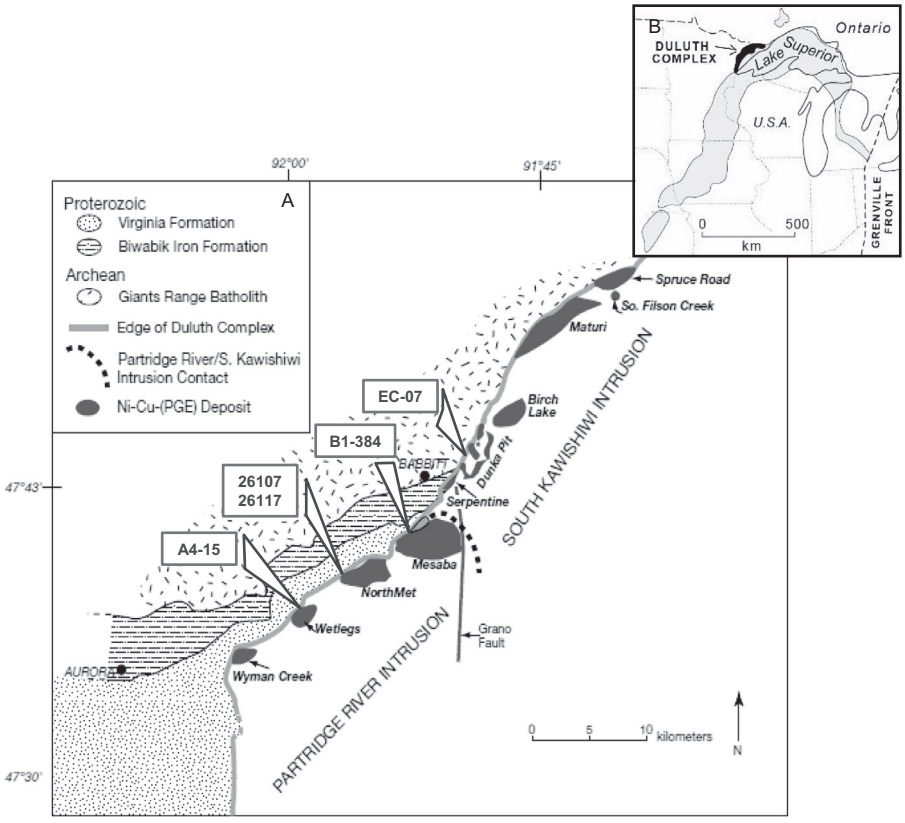


**Fig. 1.** Geological and location map of the Duluth Complex (modified from Ojakangas et al., 2001; Queffurus and Barnes, 2014; Ripley, 2014). (A) Location of the Duluth Complex in the Midcontinent Rift System (MRS). (B) Duluth Complex intrusions with locations of the diamond drill-hole cores sampled in this study.

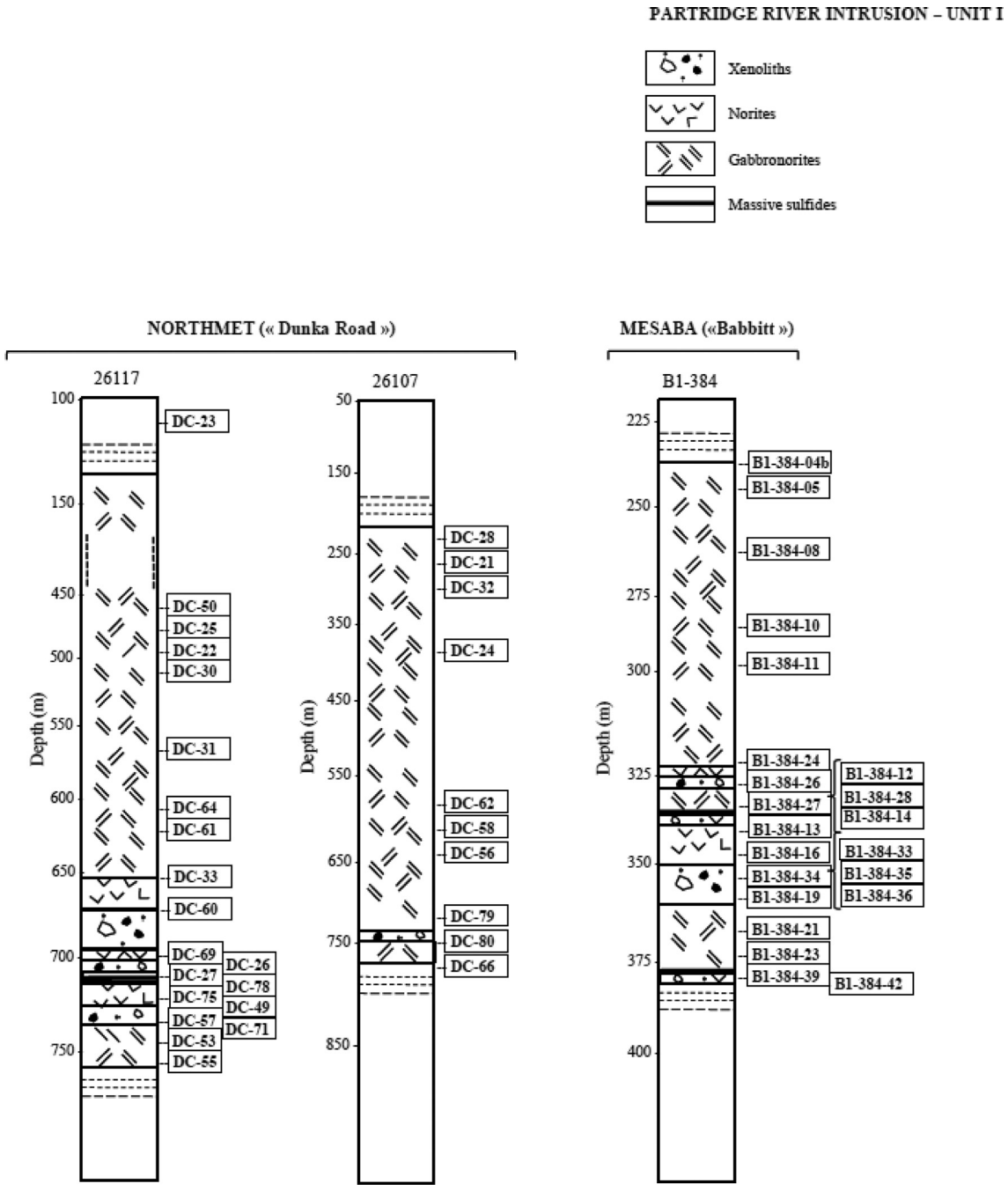


**Fig. 2.** Stratigraphic position of the samples used in this study in the borehole sections of Virginia Formation country-rocks and the basal part (Unit I) of the Partridge River Intrusion (modified from Queffurus and Barnes, 2014; Samalens et al., 2017). The few samples taken from Dunka Pit, A4 -15- and LTV mine are not indicated. Abbreviations: PRI = Partridge River intrusion, BPU = Bedded Pyrrhotite Unit.

tary rocks are essentially unmetamorphosed and the sulfide mineral present in these is pyrite (Bonnichsen, 1972; Lucente and Morey, 1983, Fig. 2A; Queffurus and Barnes, 2014). Whereas close to the intrusion in the contact aureole, the sedimentary rocks of the Virginia Formation have undergone contact metamorphism at temperature greater than 800 °C and the sulfide present in these is pyrrhotite (Labotka et al., 1981; Tracy and Frost, 1991; Sawyer, 2014).

One unit of particular interest is the Bedded Pyrrhotite Unit consisting of sulfide-rich black shales in the Virginia Formation and believed to have been deposited in restricted anoxic basins (Hauck et al., 1997). The Bedded Pyrrhotite Unit is mostly present close to the contact with the Duluth Complex (Severson and Hauck, 2008). This unit is approximately 200 m thick, but has a sporadic distribution. The basal unit of the Partridge River Intrusion (Unit I) contains numerous xenoliths of the Bedded Pyrrhotite Unit and of the Virginia Formation (Ripley and Alawi, 1988; Thériault et al., 2000; Severson and Hauck, 2008; Queffurus and Barnes, 2014).

## 3. Methodology

Samples of xenoliths of the Bedded Pyrrhotite Unit as well as norites and gabbronorites were collected from boreholes that crossed the basal Unit I of the Partridge River Intrusion at the

Dunka Pit, NorthMet, Mesaba deposits (Figs. 1 and 2). Samples of the Bedded Pyrrhotite Unit from within and outside the contact aureole were collected at the Wetlegs deposit (Fig. 1). Mineralogy and texture was documented in thirty-five polished thin sections. In addition, identification of minerals and back scattered electron imaging were carried out for a pyrite-rich sample that has a very fine grain size (~10 μm) at IOS laboratory, Chicoutimi, Québec, Canada using a scanning electron microscope (ZEISS EVO-MA15 HD 2013) equipped with a EDS-SDD spectrometer.

Whole rock analyzes were carried out in a previous study and results obtained from these analyzes are reported in Samalens et al. (2017). After a petrographic study of the textural varieties of the sulfide assemblages seventeen representative samples were selected for a more detailed investigation of the trace element contents and distribution in the sulfide minerals and silicate phases using LA-ICP-MS analyzes and chemical mapping.

Image analysis using the Image-Pro software (version 6.2) was carried out on eight thin sections to quantify the proportions of the sulfide minerals in xenoliths of the Bedded Pyrrhotite Unit. The results of the image analyzes are presented in Appendix A.

Sulfur, Se, PGE and TABS were determined on whole rock samples at LabMaTer, UQAC. Sulfur concentrations were determined by a HORIBA EMIA-220V induction furnace using the method of Bédard et al. (2008). Platinum-group elements were determined by Ni-sulfide fire assay Te-co-precipitations and ICP-MS analysis, in addition sample A4-15-01 was analyzed by isotope dilution (Savard et al., 2010). Selenium was determined by Thiol Cotton Fiber-Instrumental Neutron Activation Analysis (TCF-INAA) at LabMaTer, UQAC (Savard et al., 2006). The TABS in the black shales were determined by solution ICP-MS using a new analytical protocol specially designed for black shales (Henrique-Pinto et al., 2017) at LabMaTer; and in the gabbronorites TABS were determined by Fusion ICP-MS (Method: WRA42B) at Activation Laboratories Ltd (Actlabs), Ontario, Canada. Others trace elements were determined at Activation Laboratories Ltd (Actlabs), Ontario, Canada by Fusion ICP-MS (Method: WRA42B). Data are recapped in Appendix C and results for the certified reference materials are given in Appendix B of Samalens et al. (2017).

In-situ analyzes of the sulfide minerals were carried out by laser ablation induced coupled plasma mass spectroscopy (LA-ICP-MS) using a 7700× Agilent ICP-MS coupled with a Resolution M-50 Excimer (193 nm) ArF laser. The isotopes that were monitored are $^{34}S$; $^{57}Fe$; $^{59}Co$; $^{61}Ni$; $^{65}Cu$; $^{66}Zn$; $^{75}As$; $^{82}Se$; $^{95}Mo$; $^{101}Ru$; $^{103}Rh$; $^{105}Pd$; $^{107}Ag$; $^{108}Pd$; $^{111}Cd$; $^{118}Sn$; $^{121}Sb$; $^{125}Te$; $^{189}Os$; $^{193}Ir$; $^{195}Pt$; $^{197}Au$; $^{208}Pb$; $^{209}Bi$. The LA-ICP-MS general tuning parameters were a laser frequency of 15 Hz, a power of 5 mJ/pulse, a dwell time of 7,5 ms, a rastering speed from 5 to 10 μm/s and a fluence between 2 and 5 J/cm$^2$; specific values of these parameters are specified in the text. Lines scans across the surface of sulfides grains were made with beam sizes of 40 μm, 33 μm, 20 μm and 15 μm. The internal standard was $^{57}Fe$ for all sulfide minerals except galena, where Pb was used. The size of the galena grains (<10 μm) was too small for a galena only signal to be extracted, thus for galena the signal of the enclosing phase was subtracted and the galena results should be regarded as semi-quantitative. The machine was calibrated using the international reference materials po-727 (FeS doped with ~40 ppm PGE and Au, provided by Memorial University) and MASS-1 (a ZnFeCuS doped with ~50 ppm trace elements, provided by the USGS). The calibration was monitored using JBMSS-5a FeS doped with 50–100 ppm trace elements, provided by Prof. James Brenan (then at University of Toronto) and GSE-1 g-A a synthetic basalt glass provided by United States Geological Survey. Nickel and Cu argide interferences were corrected of on 101Ru and 103Rh using NiS and FeCuS blanks. Cadmium (108Cd) interference on $^{108}Pd$ was corrected for using $^{111}Cd$. Concentrations used for the calibration and results for the monitors are listed in Table 1. The LA-ICP-MS data is reported in Appendix B. LA-ICP-MS maps were produced for small (<50 μm) and large (>500 μm) sulfide grains with beam sizes of 5 and 44 μm respectively, frequency of 20 and 15 Hz respectively and fluence of 10 and 3 J/cm2 respectively. In addition, line scans with a beam size of 75 μm, a laser frequency of 25 Hz and a fluence of 10 J/cm$^2$ across sulfides beds and silicate matrix were made for a pyrite-rich sample that has a very fine grain size (~10 μm).

Platinum-group minerals were identified at the Centre Universitaire de Recherche sur l'Aluminium (CURAL), Université du Québec a Chicoutimi (UQAC), using a scanning electron microscope (JSM-6480LV) system equipped with an energy dispersive X-ray spectrometer. Back scattered electrons imaging and semi-quantitative analysis were carried out and data were treated with INCA software; i.e., an integrated platform for microanalysis in the electron microprobe. Voltage was fixed at 20 keV, current from ~1pA to 1μA and beam size less than 200 nm. Sulfides and metal standards (ASTIMEX) were used for scanning electron microprobe calibration (nickel silicide, antimony telluride, gallium arsenide, bismuth selenide, sphalerite, pentlandite, marcasite, galena and cuprite). Scanning electron microprobe results are reported in Table 2.

## 4. Results

### 4.1. Petrography

The modal percent of sulfide minerals present, their proportions and their morphology varies with their location and the type of host rock, i.e., the least metamorphosed black shales of the Bedded Pyrrhotite Unit, the more metamorphosed samples of Bedded Pyrrhotite Unit in the contact aureole, the xenoliths of the Bedded Pyrrhotite Unit and the mafic rocks.

#### 4.1.1. Bedded Pyrrhotite Unit from the contact aureole

The least metamorphosed black shales of the Bedded Pyrrhotite Unit are located away from the intrusion, i.e., outside the contact aureole (~3 km from the contact with the Duluth Complex). These samples contain 2–3 modal% sulfides consisting of very fine grained (<0.01 mm) pyrite that forms thin sulfide beds (<0.5 mm). A small amount (<5 modal%) of chalcopyrite and pyrrhotite are also found as sulfide beds (~100 μm thick) (Fig. 3A). In addition to sulfides, galena (<10 μm) and Sb-rich phases (<10 μm) (Fig. 3B), occur along with other heavy minerals, titanite, REE-bearing carbonates, Fe-oxide and apatite occur in thin beds (<0.2 mm). The matrix of the sulfides and heavy mineral beds consists of silicate phases, i.e., biotite, quartz, chlorite, plagioclase and graphite.

The more metamorphosed samples of Bedded Pyrrhotite Unit in the contact aureole contain ~15% sulfides in thin (3–10 mm) beds within a fine grained matrix of argillite. The sulfides consist of fine grained (0.1–0.5 mm) pyrrhotite (98 modal%) and chalcopyrite (<2 modal%) (Fig. 3C and Appendix A).

#### 4.1.2. Xenoliths of the Bedded Pyrrhotite Unit

Sulfide minerals occur in two forms in the xenoliths of the Bedded Pyrrhotite Unit. There are sulfide beds similar in width to the beds in the Bedded Pyrrhotite Unit of the contact aureole (Fig. 3D), and there are rounded sulfide droplets (~0.1 mm diameter) within pockets of former anatectic melt (Fig. 3E). Pockets of former anatectic melt, now crystallized occur in the xenoliths as a result of partial melting and consist of quartz, cordierite and feldspar patches filling space between the matrix grains (Fig. 3E).

Sulfides in the xenoliths of the Bedded Pyrrhotite Unit consist of pyrrhotite (77%), chalcopyrite (8%), cubanite (11%) and pentlandite

**Table 1**
Reference materials and in-house material used to calibrate the LA-ICP-MS. Certif. = Value on the certificate; std dev = standard deviation; IS = internal standard; n.a. = not available.

| | $^{34}$S % | $^{57}$Fe % | $^{59}$Co ppm | $^{61}$Ni % | $^{65}$Cu % | $^{66}$Zn ppm | $^{75}$As ppm | $^{82}$Se ppm | $^{95}$Mo ppm | $^{101}$Ru ppm | $^{103}$Rh ppm | $^{105/108}$Pd ppm | $^{107}$Ag ppm | $^{111}$Cd ppm | $^{118}$Sn ppm | $^{121}$Sb ppm | $^{125}$Te ppm | $^{189}$Os ppm | $^{193}$Ir ppm | $^{195}$Pt ppm | $^{197}$Au ppm | $^{208}$Pb ppm | $^{209}$Bi ppm |
|---|---|---|---|---|---|---|---|---|---|---|---|---|---|---|---|---|---|---|---|---|---|---|---|
| Ref mat used for calibration | po-727 | po-727 | MASS-1 | JB-MSS-5 | MASS-1 | MASS1 | MASS-1 | MASS-1 | MASS-1 | po-727 | po-727 | po-727 | MASS-1 | MASS-1 | MASS-1 | MASS-1 | MASS-1 | po-727 | po-727 | po-727 | po-727 | MASS-1 | MASS-1 |
| Working value | 39 | 61 | 60 | 1.05 | 13.40 | 210000 | 65 | 51 | 59 | 36.3 | 41.4 | 43.1 | 50 | 60 | 59 | 60 | 15 | 46.9 | 47.8 | 35.4 | 45.8 | 68 | 60 |
| Std dev | 0 | 0 | 10 | 0.01 | 0.05 | 5000 | 3 | 4 | 9 | 0.3 | 0.3 | 0.4 | 5 | 7 | 6 | 9 | inf val | 2.5 | 1.2 | 0.8 | 2.3 | 7 | inf val |
| source | Certif. | Certif. | Certif. | Working | Certif. | Certif. | Certif. | Certif | Certif | Certif | Certif | Certif | Certif | Certif | Certif | Certif | Certif. | Certif. | Certif. | Certif | Certif | Certif | Certif |
| Values obtained for in-house material | | | | | | | | | | | | | | | | | | | | | | | |
| *JB-MSS-5* | | | | | | | | | | | | | | | | | | | | | | | |
| Working values | 40.57 | 57 | n.a. | used | 0.021 | 13 | 63 | 48.35 | n.a. | 21.72 | 61.40 | 64.10 | 53.00 | 0.13 | 0.34 | 61.30 | 36 | 42.50 | 43.98 | 39.9 | 35.9 | 71.5 | 76.1 |
| Std dev | 0.60 | 0.90 | | to | 0.001 | 10 | 10 | 14.0 | – | 0.42 | 7.20 | 1.28 | 4.90 | 0.04 | 0.03 | 7.30 | 6 | 0.28 | 1.32 | 1 | 4.8 | 4.5 | 2.9 |
| This study average | 40.53 | IS | 0.90 | calibrate | 0.022 | 10.18 | 54.75 | 50.35 | 0.80 | 19.99 | 57.28 | 54.04 | 45.19 | 0.20 | 2.07 | 49.59 | 27.89 | 51.18 | 37.38 | 37.16 | 33.44 | 59.37 | 61.38 |
| Std dev (n = 12) | 0.39 | – | 0.55 | – | 0.010 | 4.05 | 13.92 | 9.65 | 0.33 | 1.82 | 3.43 | 3.65 | 7.39 | 0.52 | 4.49 | 5.09 | 11.00 | 6.57 | 4.10 | 2.29 | 3.11 | 6.99 | 10.17 |
| *GSE-1 g-A* | | | | | | | | | | | | | | | | | | | | | | | |
| Working values | n.a. | 9.87 | 380 | 0.04 | 0.035 | 460 | 260 | n.a. | 390 | n.a. | n.a. | n.a. | 200 | 160 | 280 | 450 | n.a. | n.a. | 120 | 30 | 7 | 378 | 320 |
| Std dev | – | 0.23 | 20 | 0.003 | 0.002 | 10 | 90 | – | 30 | – | – | – | 20 | 50 | 50 | 110 | - | - | - | - | - | 12 | 30 |
| This study average | 0.11 | IS | 263.4 | 0.04 | 0.035 | 318.30 | 291.50 | 80.81 | 347.93 | 0.07 | 32.80 | 108.08 | 144.59 | 185.23 | 282.50 | 317.33 | 177.33 | 0.07 | 13.40 | 12.09 | 7.81 | 313.88 | 254.14 |
| Std dev (n = 8) | 0.03 | – | 6.1 | 0.002 | 0.001 | 8.40 | 43.59 | 25.76 | 18.20 | 0.02 | 5.57 | 19.25 | 2.41 | 55.30 | 13.55 | 19.16 | 31.29 | 0.08 | 4.19 | 7.26 | 0.54 | 9.11 | 22.48 |

**Table 2**
Platinum-group mineral compositions determined by energy dispersive X-ray spectroscopy. Abbreviations: Eu = Euhedral; Sub = Subeuhedral; An = Anhedral; PGE = Platinum-group elements; PGM = Platinum-group minerals; Ccp = Chalcopyrite; Cb = Cubanite; Pn = Pentlandite; mid = middle.

| PGM | Host | Sample n° | Rock type | Magmatic Unit | Shape | Pd (wt%) | Pt (wt%) | Sn (wt%) | Pb (wt%) | As (wt%) | Bi (wt%) | Total (wt%) |
|---|---|---|---|---|---|---|---|---|---|---|---|---|
| Atokite | Ccp/Pn | DC-64 | PGE-rich gabbronorite | I/II | Eu | 57 | 21 | 21 | – | – | – | 99.5 |
| Paolivite | Ccp | B1-384-08 | Gabbronorite | mid I | Eu | 65 | – | 35 | – | – | – | 100 |
| Paolivite | Ccp | B1-384-08 | Gabbronorite | mid I | Eu | 66 | – | 33 | – | – | – | 99.4 |
| Paolivite | Ccp | B1-384-08 | Gabbronorite | mid I | Sub | 65 | – | 34 | – | – | – | 99.6 |
| Paolivite | Ccp | DC-64 | PGE-rich gabbronorite | I/II | Eu | 63 | – | 37 | – | – | – | 100 |
| Polarite | Cb | DC-64 | PGE-rich gabbronorite | I/II | Sub | 34 | – | – | – | – | 66 | 99.8 |
| Polarite | Silicate | DC-64 | PGE-rich gabbronorite | I/II | Sub | 37 | – | – | 8 | – | 55 | 99.9 |
| Zyageintsevite | Silicate | DC-64 | PGE-rich gabbronorite | I/II | Eu | 65 | – | – | 36 | – | – | 100 |
| Zyageintsevite | Cb | DC-64 | PGE-rich gabbronorite | I/II | An | 63 | – | – | 37 | 0.1 | – | 99.7 |
| Zyageintsevite | Ccp | DC-64 | PGE-rich gabbronorite | I/II | Sub | 65 | – | – | 35 | 0.1 | – | 99.7 |

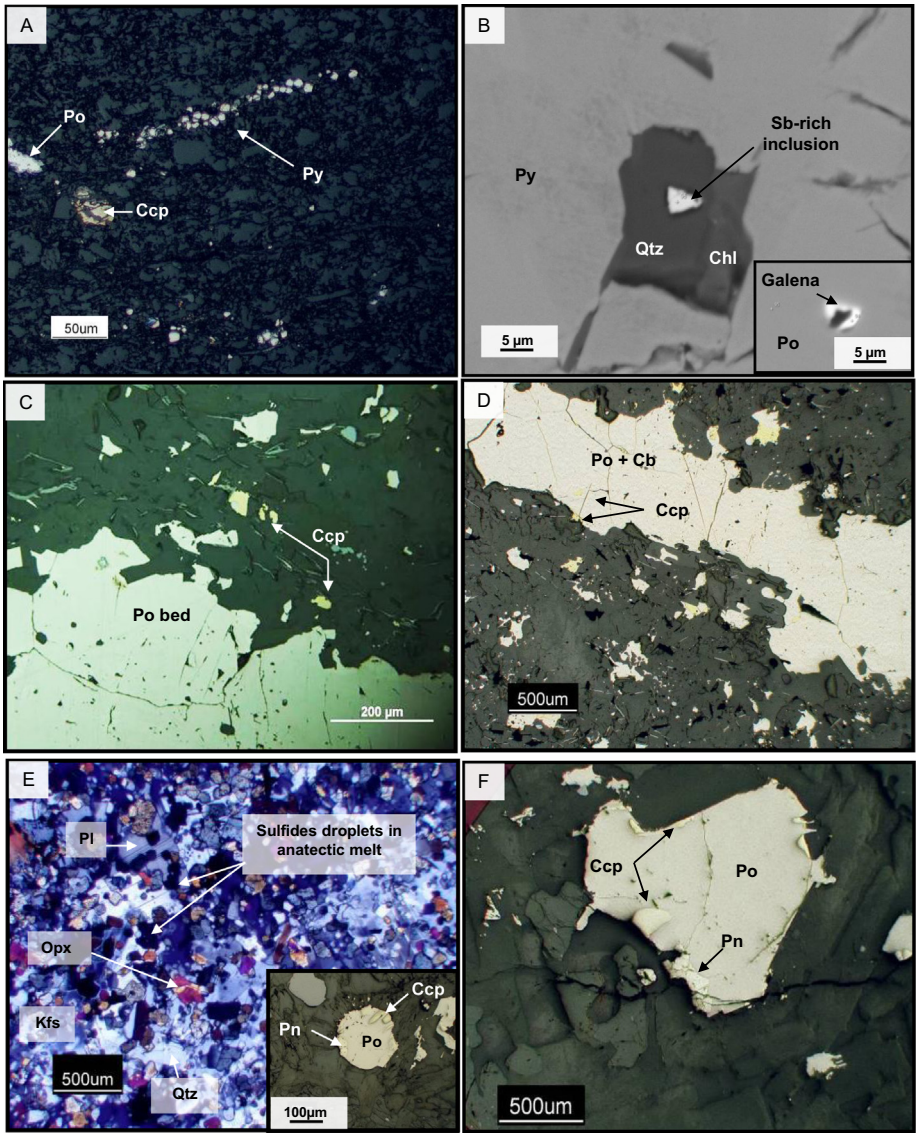


**Fig. 3.** Photomicrographs of sulfide textures in the least metamorphosed Bedded Pyrrhotite Unit (BPU) from outside the contact aureole, in the contact aureole, from BPU xenoliths and the mafic magma surrounding the BPU xenoliths. (A) Pyrite bed in the least metamorphosed BPU from outside the contact aureole. (B) Back scattered electrons image of Sb-rich phase included in a quartz grain. The right inset shows details of a galena inclusion in a pyrrhotite grain. (C) Sulfide bed in the BPU from the contact aureole. (D) Sulfide bed within a BPU xenolith. (E) Partial melting texture in a BPU xenolith. The right inset shows details of a sulfide droplet in the anatectic melt. (F) Sulfide droplet within mafic magma (norite). Abbreviations: Silicates: Chl = Chlorite; Opx = Orthopyroxene; Pl = Plagioclase; Kfs = K-Feldspar; Qtz = Quartz. Sulfides: Ccp = Chalcopyrite; Cb = Cubanite; Po = Pyrrhotite; Pn = Pentlandite, Py = Pyrite.

(4%). There is a greater proportion of Cu-rich sulfides (chalcopyrite and cubanite) and pentlandite (~25% and 2–15% respectively) than observed in the contact aureole (Appendix A). The samples contain 10–30 modal% sulfides.

#### 4.1.3. Mafic rocks

The groundmass in the norites and gabbronorites contains disseminated droplets of sulfide (~100 μm to 1 mm) (Fig. 3F). Norites have the same sulfide assemblage as the Bedded Pyrrhotite Unit xenoliths, but with a slightly lower percentage of pentlandite (<5% modal) and cubanite (~5–10%), whereas the sulfide mineral assemblages in the gabbronorites contain more chalcopyrite, cubanite and pentlandite but less pyrrhotite (<20% modal).

#### 4.1.4. Platinum-group minerals

In our samples, platinum-group minerals were only found in gabbronorites from the magmatic units I and II. The platinum-group minerals were found within base metal sulfide grains, at the rim of sulfide grains and filling fractures within the sulfide minerals (Fig. 4A–F). A total of ten platinum-group mineral grains (<5 μm) were identified in the disseminated sulfides (Table 2). The platinum-group minerals present are polarite (Pd-Bi), paolivite ($Pd_2Sn$), zvyageintsevite $Pd_3Pb$ and atokite $(Pd, Pt)_3Sn$.

### 4.2. Geochemistry

#### 4.2.1. Elements concentrated in pyrrhotite and pentlandite

Cobalt content provides a convenient way of separating the base metal sulfide minerals on bivariate plots such as Co versus Ni (Fig. 5A) because Co is present in all the minerals and has a low detection limit (Table 3 and Appendix B). Cobalt concentrations are the highest in pentlandite ranging from 0.3 to 3 wt%. Cobalt concentrations in pentlandite from the xenoliths plot at the high end of this range. Pyrrhotite contains from 10 to

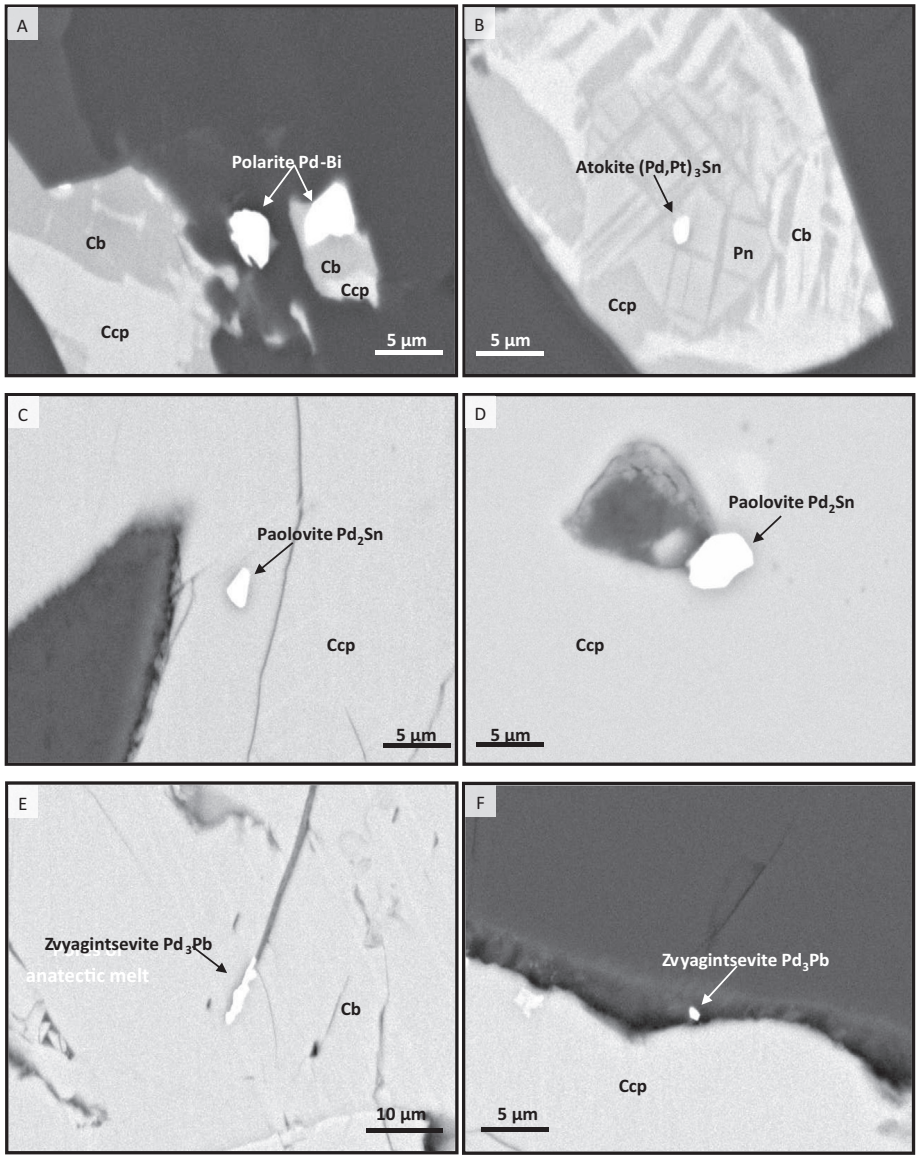


**Fig. 4.** Backscattered electron images of Platinum Group Minerals (PGM) hosted by chalcopyrite and cubanite sulfides from gabbronorites of the basal Unit I and II. (A) Polarite (Pd-Bi) grain in cubanite. (B) Atokite [$(Pd, Pt)_3Sn$] grain in cubanite. (C) and (D) Paolovite ($Pd_2Sn$) grains hosted by chalcopyrite. (E) Zvyagintsevite ($Pd_3Pb$) grain hosted by chalcopyrite. Zvyagintsevite grains fill fractures in chalcopyrite. (F) Zvyagintsevite ($Pd_3Pb$) grain at the rim of a chalcopyrite grain. Abbreviations: Cb = Cubanite; Ccp = Chalcopyrite.

200 ppm Co, with the pyrrhotite from the Bedded Pyrrhotite Unit in the contact aureole having the highest contents. Pyrite in the least metamorphosed Bedded Pyrrhotite Unit from outside the contact aureole contains similar Co contents to pyrrhotite from the contact aureole. Chalcopyrite and cubanite from the mafic rocks generally contain the lowest concentration of Co ranging from 0.01 to 20 ppm, whereas chalcopyrites from xenoliths of the Bedded Pyrrhotite Unit and the least metamorphosed Bedded Pyrrhotite Unit from outside the intrusion contain slightly more Co, from 1 to 100 ppm.

Pentlandite is the base metal sulfide which has the highest Ni, Pd and Rh concentrations (only Ni and Pd are shown in the Fig. 5A and B). Palladium and Rh concentrations in pentlandite range respectively from 0.1 to 3 ppm and 0.005 to 0.5 ppm (only Pd vs. Co is shown in Fig. 5B). Pyrite in the least metamorphosed Bedded Pyrrhotite Unit from outside the contact aureole contains ~0.3 ppm Pd (Fig. 5B), values which are similar to the pentlandite of other rock types, and ~0.08 ppm Rh (Table 3 and Appendix B). Pyrrhotite from all rock types contains a little Pd, from ~0.01 to 0.1 ppm and between 0.003 and 0.02 ppm Rh. For most chalcopyrites and cubanites Pd concentrations are less than detection limit and concentrations of Rh could not be determined because of the Cu interference on Rh. However, the chalcopyrite from the contact aureole contains significant amounts of Pd (~0.8 to 2 ppm). The isotope $^{108}Pd$ was used to calculate the amount of Pd present, thus this value is not a product of Cu interference. Furthermore, cadmium levels are low (<2 ppm) in these chalcopyrites, thus the $^{108}Cd$ interference is insignificant. Therefore, the high Pd content in these chalcopyrites is not thought to be an artefact.

Arsenic concentrations are generally highest in pentlandite and values are ~1 to 10 ppm, and the lowest in cubanite and chalcopyrite which have concentrations of only 0.08 to 2 ppm (Fig. 5C). Pyrrhotite generally contains intermediate values ranging from ~0.1 to 10 ppm. An exception to this is pyrrhotite in the least metamorphosed Bedded Pyrrhotite Unit from outside the contact aureole which has the highest As contents of ~20 ppm.

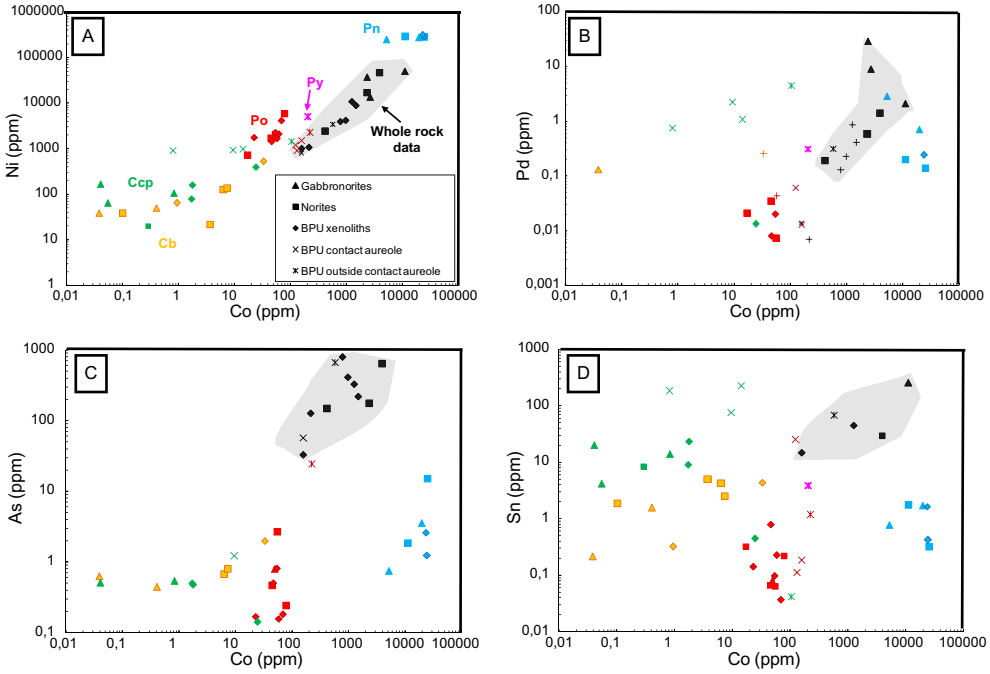


**Fig. 5.** Plots of (A) Ni, (B) Pd, (D) As and (E) Sn vs. Co in the Bedded Pyrrhotite Unit (BPU) rocks and the mafic magma. Averages of Ni, Pd, As and Sn content of sulfide minerals are compared to trace metal contents of the sulfide component in the whole-rock recalculated to 100% sulfides. Field of the whole-rock concentrations is shaded in grey. Abbreviation: BPU = Bedded Pyrrhotite Unit.

Molybdenum concentrations are the highest in the pyrrhotite from the Bedded Pyrrhotite Unit from the contact aureole and pyrite from the least metamorphosed Bedded Pyrrhotite Unit outside the contact aureole, and lie between ~0.5 and 100 ppm (Table 3 and Appendix B). Pyrrhotite from the other rock types contain intermediate concentrations of Mo (~0.1 to 4 ppm). Pentlandite is generally poor in Mo with values from 0.02 to 0.3 ppm. Most of the cubanite and chalcopyrite are very poor in Mo (~0.01 to 0.1 ppm). However, an exception to this is the chalcopyrite from the contact aureole which is slightly richer at ~0.1 to 1 ppm.

*4.2.2. Elements concentrated in Cu-rich sulfides*

Some elements, Cu, Sn, Zn, Ag, Cd and to a lesser extent Pb and Sb are concentrated in chalcopyrite and cubanite (only Sn, Pb and Sb vs. Co are shown in Fig. 5D; Fig. 6A and B; Table 3 and Appendix B). For most of these trace elements, the tendency for the pyrite and pyrrhotite in the least metamorphosed Bedded Pyrrhotite Unit from outside the contact aureole to be richer in trace elements than the other pyrrhotites is evident.

The concentrations of Sn and Ag are the highest in chalcopyrite from the rocks inside and outside the intrusion, respectively 80–200 ppm and 40–300 ppm (only Sn vs. Co is shown in Fig. 5D). Pentlandite contains slightly lower Ag and Sn contents than chalcopyrite, or cubanite, generally ~0.3 to 10 ppm and ~0.02 to 2 ppm respectively. The pentlandite in the xenoliths contains less Ag and Sn than the pentlandite from the mafic rocks. Most of the pyrrhotites contain less Ag or Sn (0.03–2 ppm) than the other minerals. However, pyrrhotite and pyrite in the least metamorphosed Bedded Pyrrhotite Unit from outside the contact aureole are an exception to this, and contain high Ag and Sn levels (respectively ~10 to 30 ppm and ~5 to 20 ppm).

Lead concentrations are generally higher in the chalcopyrite and cubanite (~1 to 40 ppm) from the mafic rocks and xenoliths than in the pyrrhotite (~ 0.1 to 2 ppm) and the pentlandite (~ 1 to 10 ppm) regardless of the rock type. Pyrrhotite and pyrite from the contact aureole and from outside the contact aureole have the highest Pb contents at ~100 to 1000 ppm (Fig. 6A). Pentlandite contains intermediate levels of Pb with values between ~1 and 10 ppm.

Antimony concentrations are the highest in the chalcopyrite from the Bedded Pyrrhotite Unit of the contact aureole and in the pyrite and pyrrhotite in the least metamorphosed Bedded Pyrrhotite Unit from outside the contact aureole (~10–100 ppm) (Fig. 6B). All the base metal sulfides from the xenoliths have very low Sb concentrations generally around 0.02 to 1 ppm. The concentrations of Sb in base metal sulfides from the mafic rocks are less than detection levels (0.02 ppm).

*4.2.3. Elements present in all base metal sulfides*

Selenium, Te and Bi are present in approximately equal amounts in all the sulfide minerals (Table 3, Appendix B; only Te and Bi vs. Co are shown in Fig. 6C and D). The sulfides in the mafic rocks tend to be the richest in Se and Te (respectively 40–100 ppm and 1–20 ppm). The chalcopyrite and pyrrhotite in the contact aureole are the poorest in Se and Te (respectively, 10–20 ppm and below the detection limit). The pyrite and pyrrhotite outside the contact aureole have the highest Se contents (~100 to 200 ppm). Bismuth occurs in approximately equal amounts in all the sulfide minerals and concentrations are in the range of 0.1–5 ppm.

*4.2.4. Elements in galena*

The mineral richest in the TABS is the galena found in the Bedded Pyrrhotite Unit from outside the contact aureole. Small grains of galena are present in narrow heavy mineral beds. Galena contains Ag, Cd, Sn, Sb and Bi in the 0.1–0.5 wt% range (Table 3) and also contains significant amounts of Te (~200 ppm).

*4.2.5. Recalculation to 100% sulfides*

The concentrations of the elements in the whole rocks recalculated to 100% sulfides (based on Eq. (1) in Barnes and Lightfoot, 2005) are shown on Figs. 5 and 6 for Ni, Pd, As, Sn, Pb, Sb, Te, Bi

**Table 3**
Concentrations of chalcophile elements in base metal sulfide minerals from the Partridge River Intrusions determined by LA-ICP-MS. Abbreviations: n = number of analysis; Py = Pyrite; Po = Pyrrhotite; Pn = Pentlandite; Ccp = Chalcopyrite; Cb = Cubanite; BPU = Bedded Pyrrhotite Unit; c.a. = contact aureole; AM = Arithmetic mean.

| | n | Sulfide | Sample n° | Rock type | Sulfide texture | Co (ppm) | Ni (ppm) | Cu (ppm) | Zn (ppm) | As (ppm) | Se (ppm) | Mo (ppm) | Ru (ppm) | Rh (ppm) | Pd (ppm) | Ag (ppm) | Cd (ppm) | Sn (ppm) | Sb (ppm) | Te (ppm) | Os (ppm) | Ir (ppm) | Pt (ppm) | Au (ppm) | Pb (ppm) | Bi (ppm) |
|---|---|---|---|---|---|---|---|---|---|---|---|---|---|---|---|---|---|---|---|---|---|---|---|---|---|
| AM | 2 | Ccp | LTV-7555 | BPU outside c.a. | Sulfide bed | 105 | 1421 | 299494 | 200 | – | 77.96 | 1.50 | 0.41 | n.d. | 4.45 | 282.78 | 1.32 | 0.04 | 6.71 | – | 0.004 | 0.019 | – | – | 40.29 | – |
| AM | 2 | Po | LTV-7555 | BPU outside c.a. | Sulfide bed | 226 | 2278 | 742 | 1097 | 24.31 | 141.49 | 122.79 | n.d. | 0.075 | – | 26.61 | 22.59 | 1.18 | 140.55 | – | – | 0.034 | – | – | 646.99 | – |
| AM | 3 | Py | LTV-7555 | BPU outside c.a. | Sulfide bed | 205 | 5024 | 673 | 317 | – | 129.88 | 8.69 | n.d. | 0.075 | 0.31 | 17.67 | 14.70 | 3.83 | 13.09 | – | – | 0.019 | – | – | 80.35 | – |
| AM | 4 | Ga* | LTV-7555 | BPU outside c.a. | Heavy mineral | 11933 | – | – | – | – | 80 | – | – | – | – | 5623 | 826 | 3310 | 4637 | 262 | – | – | – | – | IS | 2310 |
| AM | 2 | Ccp | A4-15-01 | BPU c.a | Sulfide bed | 0.8 | 899 | 380983 | 316 | – | 11.65 | 0.50 | 0.39 | – | 0.74 | 45.25 | 2.10 | 183.49 | 15.17 | 0.09 | – | – | – | – | 10.25 | 0.92 |
| AM | 4 | Ccp | A4-15-01 | BPU c.a | Sulfide droplet IM | 14 | 861 | 379544 | 304 | – | 17.28 | 0.18 | 0.38 | – | 1.08 | 62.44 | 1.53 | 224.17 | 4.01 | – | – | 0.021 | – | – | 16.13 | – |
| – | 1 | Ccp | DC-70 | BPU c.a | Sulfide bed | 10 | 919 | 351162 | 350 | 1.22 | 13.21 | 0.48 | 0.20 | – | 2.22 | 129.63 | 1.95 | 74.86 | 6.33 | 0.40 | – | – | – | – | 31.65 | 1.70 |
| AM | 2 | Po | A4-15-01 | BPU c.a | Sulfide droplet IM | 126 | 1183 | 2.0 | 0.7 | – | 14.27 | 0.65 | – | 0.011 | 0.06 | 1.08 | 0.08 | 24.93 | 0.75 | – | – | – | – | – | 8.87 | 1.00 |
| AM | 4 | Po | A4-15-01 | BPU c.a | Sulfide bed | 133 | 900 | 4.0 | 1.0 | – | 14.71 | 0.65 | 0.06 | – | – | 0.86 | – | 0.11 | 1.68 | – | – | – | – | – | 4.22 | 0.33 |
| AM | 3 | Po | DC-70 | BPU c.a | Sulfide bed | 159 | 1490 | 6.0 | 0.8 | – | 14.54 | 0.49 | – | – | 0.01 | 0.17 | 0.03 | 0.18 | – | – | – | – | – | – | 3.32 | 1.52 |
| – | 1 | Ccp | DC-69 | BPU xenoliths | Sulfide droplet | 25 | 396 | 292432 | 190 | 0.14 | 27.87 | 0.31 | 0.06 | – | 0.01 | 0.83 | 4.56 | 0.45 | 0.15 | 0.32 | 0.028 | 0.027 | – | – | 9.07 | 1.10 |
| – | 1 | Ccp | DC-80 | BPU xenoliths | Sulfide droplet | 1.8 | 158 | 309777 | 593 | 0.47 | 54.10 | 0.03 | 0.08 | – | – | 2.08 | 16.13 | 22.97 | 0.07 | 12.20 | – | – | – | – | 5.72 | 0.47 |
| AM | 3 | Ccp | EC-07 | BPU xenoliths | Sulfide droplet | 1.7 | 78 | 306430 | 1238 | 0.49 | 38.74 | 0.02 | 0.08 | – | – | 3.38 | 38.91 | 8.93 | 0.46 | 4.06 | – | 0.003 | – | 0.049 | 15.64 | 1.01 |
| AM | 8 | Cb | B1-384-26 | BPU xenoliths | Sulfide bed | 33 | 527 | 217061 | 1163 | 1.97 | 30 | 1.5 | 0.15 | – | 0.25 | 10.0 | 8.39 | 4.33 | 0.02 | 7.0 | – | – | – | 0.02 | 14.09 | 1.59 |
| – | 1 | Cb | B1-384-39 | BPU xenoliths | Sulfide droplet | 1.0 | 65 | 213157 | 32 | – | 32.22 | 0.01 | 0.20 | – | – | 5.19 | 4.28 | 0.32 | – | 1.56 | – | – | – | – | 5.14 | – |
| AM | 5 | Pn | B1-384-26 | BPU xenoliths | Sulfide bed | 24199 | 285486 | 84.9 | 12 | 1.23 | 23 | 0.3 | – | 0.04 | 0.24 | 1.0 | 0.05 | 0.42 | 0.39 | 1.8 | 0.02 | – | – | 0.01 | 4.35 | 1.74 |
| AM | 2 | Pn | DC-80 | BPU xenoliths | Sulfide droplet | 23541 | 319739 | 2.8 | 108 | 2.58 | 44.85 | 0.12 | – | – | 0.24 | 2.55 | 2.21 | 1.61 | 0.42 | 7.59 | | – | – | 0.029 | 5.29 | 3.01 |
| AM | 13 | Po | B1-384-26 | BPU xenoliths | Sulfide bed | 58 | 1657 | 252.5 | 7 | 0.15 | 34 | 0.7 | 0.03 | 0.01 | 0.04 | 0.2 | 0.06 | 0.23 | – | 0.6 | – | 0.001 | 0.02 | 0.002 | 0.57 | 0.82 |
| AM | 4 | Po | B1-384-26 | BPU xenoliths | Sulfide bed | 46 | 1426 | 3.8 | 92 | 0.50 | 56 | 0.4 | 0.05 | – | 0.01 | 0.3 | 0.07 | 0.78 | – | – | 0.03 | – | – | – | 0.49 | 1.71 |
| AM | 3 | Po | DC-71 | BPU xenoliths | Sulfide bed | 23 | 1742 | 8.4 | 0 | 0.17 | 30 | 0.5 | 0.02 | – | – | 0.2 | 0.04 | 0.14 | 0.03 | – | – | – | – | – | 0.83 | 0.14 |
| – | 1 | Po | B1-384-39 | BPU xenoliths | Sulfide droplet | 62 | 2092 | 1.2 | 0.1 | – | 26.24 | 0.92 | 0.13 | – | – | 0.30 | – | – | – | – | 0.037 | – | – | – | 0.17 | – |
| – | 1 | Po | DC-69 | BPU xenoliths | Sulfide droplet | 69 | 4132 | 0.7 | 0.2 | 0.18 | 29.11 | 0.06 | 0.10 | 0.005 | – | 0.04 | 0.08 | 0.04 | 0.02 | – | – | – | – | – | 0.36 | 0.11 |
| AM | 4 | Po | DC-80 | BPU xenoliths | Sulfide droplet | 54 | 2252 | 0.6 | 0.7 | 0.81 | 38.97 | 0.42 | 0.03 | 0.003 | 0.02 | 0.09 | 0.01 | 0.10 | 0.03 | – | – | – | – | – | 0.58 | 0.24 |
| – | 1 | Ccp | B1-384-39 | Massive sulfides | Massive sulfides | 0.5 | 11 | 307343 | 697 | 0.08 | 35.60 | 0.03 | 0.10 | – | – | 1.68 | 13.82 | 0.27 | – | 2.44 | – | – | – | – | 0.99 | 0.11 |
| AM | 5 | Ccp | DC-69 | Massive sulfides | Massive sulfides | 2.0 | 55 | 311135 | 275 | 0.17 | 32.80 | 0.06 | 0.08 | – | – | 0.49 | 11.37 | 3.83 | 0.03 | 3.72 | – | – | – | 0.006 | 6.03 | 0.30 |
| AM | 2 | Cb | B1-384-39 | Massive sulfides | Massive sulfides | 0.9 | 19 | 210688 | 3086 | – | 24.83 | 0.01 | 0.13 | – | – | 5.52 | 71.60 | 0.10 | – | 0.99 | – | – | – | – | 0.88 | 0.08 |
| – | 1 | Pn | B1-384-26 | Massive sulfides | Massive sulfides | 26992 | 307041 | 2.2 | 0.29 | 1.99 | 38.10 | 0.31 | – | 0.007 | 0.41 | 1.10 | 0.01 | 0.40 | – | 0.33 | – | – | – | – | 1.42 | 1.37 |
| – | 1 | Pn | B1-384-39 | Massive sulfides | Massive sulfides | 10618 | 294668 | 1.3 | 0.32 | – | 18.79 | 0.04 | – | – | 1.00 | 1.76 | 0.01 | 0.01 | – | – | – | – | – | – | 0.07 | – |
| AM | 3 | Pn | DC-69 | Massive sulfides | Massive sulfides | 27209 | 363153 | 10.7 | 0.71 | 3.20 | 25.42 | 0.34 | – | 0.012 | 1.30 | 0.39 | 0.03 | 0.04 | 0.13 | – | – | – | – | 0.007 | 1.79 | 0.32 |
| AM | 3 | Po | B1-384-26 | Massive sulfides | Massive sulfides | 45 | 1587 | 18.8 | 0.97 | – | 51.42 | 0.81 | 0.06 | 0.007 | – | 0.50 | 0.05 | 0.21 | – | 0.62 | 0.03 | – | – | – | 0.67 | 1.76 |
| AM | 6 | Po | B1-384-39 | Massive sulfides | Massive sulfides | 48 | 1640 | 4.5 | 0.33 | 0.12 | 25.46 | 0.61 | 0.12 | 0.009 | 0.10 | 0.23 | 0.04 | 0.05 | – | – | 0.04 | – | – | 0.014 | 0.26 | 0.06 |
| AM | 2 | Po | DC-69 | Massive sulfides | Massive sulfides | 247 | 6878 | 9.6 | 0.21 | 0.32 | 27.74 | 1.17 | 0.23 | 0.010 | 0.03 | 0.11 | 0.02 | 0.04 | 0.03 | – | – | – | – | – | 0.39 | 0.09 |
| – | 1 | Po | DC-71 | Massive sulfides | Massive sulfides | 23 | 1852 | 223 | 3.68 | 13.96 | 29.73 | 0.39 | 0.01 | 0.006 | – | 0.24 | 0.05 | 0.13 | – | – | – | – | – | – | 1.40 | 0.13 |
| AM | 3 | Ccp | B1-384-12 | Norite | Sulfide droplet | 0.3 | 20 | 316269 | 270 | – | 66.41 | – | 0.29 | – | – | 5.88 | 18.39 | 8.35 | – | 4.17 | – | – | – | – | 2.45 | 1.52 |
| AM | 5 | Cb | B1-384-12 | Norite | Sulfide droplet | 3.7 | 21 | 219988 | 1878 | – | 72.05 | 0.01 | 0.22 | – | – | 44.28 | 104.85 | 5.01 | – | 6.39 | – | – | – | – | 9.93 | 1.06 |
| AM | 2 | Cb | B1-384-13 | Norite | Sulfide droplet | 6.3 | 126 | 222128 | – | 0.67 | 81.11 | 0.06 | 0.26 | – | – | 7.44 | 9.53 | 4.22 | – | 14.01 | – | – | – | – | 17.74 | 0.11 |
| AM | 3 | Cb | B1-384-16 | Norite | Sulfide droplet | 7.4 | 137 | 222622 | – | 0.79 | 60.44 | 0.05 | 0.23 | – | – | 11.74 | 27.98 | 2.48 | – | 14.64 | – | – | – | – | 11.84 | 0.43 |
| AM | 3 | Cb | B1-384-21 | Norite | Sulfide droplet | 0.1 | 39 | 221291 | – | – | 55.53 | – | 0.26 | – | – | 6.53 | 6.99 | 1.86 | – | 1.82 | – | – | – | – | 26.34 | 0.26 |
| – | 1 | Pn | B1-384-13 | Norite | Sulfide droplet | 25136 | 281318 | 27 | – | 14.98 | 65.45 | 0.08 | – | 0.007 | 0.14 | 11.23 | 63.49 | 0.32 | 0.45 | 18.69 | 0.026 | – | – | – | 10.32 | 1.79 |
| AM | 3 | Pn | B1-384-21 | Norite | Sulfide droplet | 11233 | 290652 | 4906 | – | 1.83 | 40.09 | 0.07 | – | 0.475 | 0.20 | 6.63 | 0.09 | 1.75 | – | 1.56 | 0.031 | – | – | – | 19.46 | 0.13 |
| AM | 5 | Po | B1-384-13 | Norite | Sulfide droplet | 55 | 1992 | 8 | – | 2.66 | 64.45 | 1.89 | 0.05 | 0.006 | 0.01 | 0.24 | 0.33 | 0.06 | – | – | 0.038 | – | – | – | 0.31 | 0.32 |
| AM | 5 | Po | B1-384-16 | Norite | Sulfide droplet | 45 | 1708 | 14 | – | 0.46 | 46.64 | 1.07 | 0.05 | 0.005 | 0.03 | 0.33 | 0.05 | 0.07 | – | – | – | – | – | – | 0.46 | 0.63 |
| AM | 4 | Po | B1-384-21 | Norite | Sulfide droplet | 17 | 726 | 94 | – | – | 45.22 | 0.61 | 0.09 | 0.022 | 0.02 | 0.59 | 0.08 | 0.32 | – | – | 0.065 | – | – | – | 0.40 | 0.38 |
| – | 1 | Po | EC-07 | Norite | Sulfide droplet | 79 | 5778 | 11 | 1.0 | 0.24 | 38.27 | 2.31 | 0.03 | 0.013 | – | 0.17 | 0.07 | 0.22 | – | – | 0.005 | 0.005 | – | – | 1.48 | 0.13 |
| AM | 2 | Ccp | B1-384-04B | Gabbronorite | Sulfide droplet | 0.8 | 105 | 324992 | – | 0.54 | 38.22 | – | 0.35 | – | – | 2.39 | 20.53 | 13.83 | – | 3.99 | – | – | – | – | 3.01 | – |
| AM | 2 | Ccp | B1-384-05 | Gabbronorite | Sulfide droplet | 0.04 | 165 | 333361 | – | 0.51 | 106.35 | 0.05 | 0.38 | – | – | 5.40 | 3.57 | 19.92 | – | 1.58 | – | – | – | – | 4.46 | – |
| AM | 2 | Ccp | B1-384-08 | Gabbronorite | Sulfide droplet | 0.06 | 64 | 331231 | – | – | 92.84 | – | 0.33 | – | – | 8.44 | 5.86 | 4.12 | – | 1.63 | – | – | – | – | 3.31 | – |
| AM | 3 | Cb | B1-384-04B | Gabbronorite | Sulfide droplet | 0.41 | 50 | 223321 | – | 0.44 | 36.97 | 0.03 | 0.24 | – | – | 9.72 | 10.00 | 1.55 | – | 4.91 | – | – | – | – | 8.85 | 0.06 |
| AM | 3 | Cb | B1-384-08 | Gabbronorite | Sulfide droplet | 0.04 | 38 | 232991 | – | 0.62 | 96.54 | 0.03 | 0.22 | – | 0.13 | 20.90 | 22.59 | 0.21 | – | 1.77 | – | – | – | – | 22.44 | – |
| – | 1 | Pn | B1-384-04B | Gabbronorite | Sulfide droplet | 19796 | 274481 | 1.1 | – | 3.55 | 28.42 | 0.25 | – | – | 0.71 | 1.68 | 0.07 | 1.69 | 0.21 | 0.68 | – | – | – | – | 2.31 | 0.04 |
| AM | 2 | Pn | B1-384-08 | Gabbronorite | Sulfide droplet | 5245 | 248921 | 674 | – | 0.74 | 84.82 | 0.04 | – | 0.087 | 2.85 | 128.90 | 0.35 | 0.76 | – | 1.47 | 0.035 | – | – | – | 8.58 | 0.10 |
| AM | 5 | Po | B1-384-04B | Gabbronorite | Sulfide droplet | 50 | 1898 | 8 | – | 0.79 | 32.59 | 3.58 | 0.07 | 0.007 | – | 0.29 | 0.05 | 0.08 | 0.02 | 0.20 | – | – | – | – | 0.41 | 0.43 |

*Ga = Galena semi-quantitive.

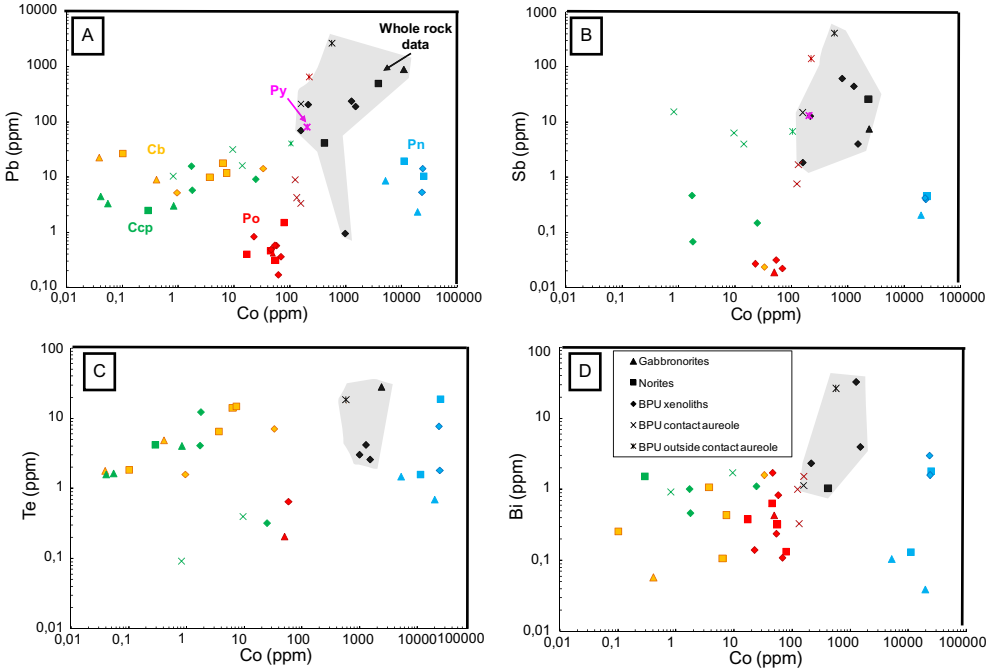


**Fig. 6.** Plots of (A) Pb, (B) Sb, (C) Te and (D) Bi vs. Co in the Bedded Pyrrhotite Unit (BPU) rocks and the mafic magma. Averages of Pb, Sb, Te and Bi content of sulfide minerals are compared to trace metal contents of the sulfide component in the whole-rock recalculated to 100% sulfides. Field of the whole-rock concentrations is shaded in grey. Abbreviation: BPU = Bedded Pyrrhotite Unit.

and Table 4. These concentrations are similar to the concentrations found in the base metal sulfide minerals for Ni, Cu, Co, Rh, Pd, Se and Te indicating that these elements are present mainly in the sulfides in these rocks. In contrast, Mo, As, Zn, Ag, Sn, Pb, Sb and Bi concentrations in the base metal sulfides are lower than in the whole rock recalculated to 100% sulfides, which indicates that these elements must also be present in some other phases in the rocks. Note that whole rock data for Cd are not available.

*4.2.6. Line scans across sulfides of the Bedded Pyrrhotite Unit from outside the contact aureole*

Line scans across the sulfide beds, i.e., pyrite- and pyrrhotite-rich beds, using a 75 μm beam showed that most chalcophile elements are concentrated in the sulfide beds by one to three orders of magnitude in comparison with the matrix (Fig. 7). Note that a 75 μm beam size was chosen in order to better reduce the detection limits for these elements. The calculated averages of the contents of Sn, Sb, Pb, Bi, Ag, Cu and Te of the sulfide beds are respectively ~1 ppm, 1500 ppm, 50 ppm, 4 ppm, 350 ppm, 30 ppm and 10 ppm.

Metal contents of the pyrites and sulfide beds normalized to whole rock are shown in the Fig. 8. Nickel, Co, Rh and Pd are enriched in the pyrites relative to the whole rock by one order of magnitude, the pyrite content of the rocks is 1–2% and thus pyrite could be the main host of these elements in the black shale. However, most of the other chalcophile elements are present in the pyrite at only approximately the same levels as the whole rock thus some other phase(s) must host these elements.

*4.2.7. Chemical maps*

Chemical maps of the trace element in pyrrhotite-rich sulfide beds of the least metamorphosed Bedded Pyrrhotite Unit from outside the contact aureole using a smaller beam size (5 μm) showed that Sb and Bi are concentrated in the chalcopyrite relative to pyrrhotite and the silicate matrix, and that Pb is present both in the sulfides and the silicate matrix (Fig. 9). No enrichments in Te and As were observed, possibly because the concentrations are too low to be observed with a 5 μm beam, and possibly because there was no pyrite present in the mapped area.

Sulfide droplets trapped within the anatectic melt of the xenoliths of the Bedded Pyrrhotite Unit contain TABS and these elements are concentrated in the same area where grains of pentlandite and chalcopyrite occur (Fig. 10). In contrast, Pb is found mainly in plagioclase, although there is some Pb associated with the Cu-rich sulfides.

In sulfide droplets from the gabbronorites and norites most of the TABS are associated with pentlandite and Cu-rich sulfides but are absent in silicate phases (Figs. 11 and 12). In contrast, Pb is present both in the silicate matrix surrounding the sulfides (plagioclases) and in the sulfides (Fig. 11). Tin is partitioned between Cu-rich sulfides and pyroxene. Sulfide droplets in the norite and gabbronorites have TABS-rich clusters that also contain PGE, as shown for Pd in Figs. 11 and 12.

## 5. Discussion

### 5.1. TABS-hosted minerals in the Duluth Complex

*5.1.1. Bedded Pyrrhotite Unit from the contact aureole, Bedded Pyrrhotite Unit xenoliths and mafic rocks*

Most of the TABS are associated with Cu-rich sulfides and pentlandite in the Bedded Pyrrhotite Unit from the contact aureole, the Bedded Pyrrhotite Unit xenoliths and the mafic rocks of the Duluth Complex. Numerous authors have shown that the base metal sulfides and accessory PGM associated with the base metals sulfides host much of the chalcophile element budgets in magmatic Ni-Cu-PGE deposits (Barnes et al., 1997; Godel et al., 2007; Holwell and McDonald, 2007; Hutchinson and McDonald, 2008; Dare et al., 2010,2011; Piña et al., 2012; Osbahr et al., 2013; Chen et al., 2015; Duran et al., 2016). The TABS are not strongly chalcophiles in comparison with PGE (Table 1 in Barnes and Ripley, 2016 and references therein). Chalcophile elements partition into

**Table 4**
Whole-rock compositions of the Bedded Pyrrhotite Unit from the contact aureole, the Bedded Pyrrhotite Unit xenoliths, the norites and the gabbronorites of the Partridge River Intrusion. Abbreviations: BPU = Bedded Pyrrhotite Unit; c.a. = contact aureole; n.d. = not determined.

| | Sample | Rock type | S (%) | Co (ppm) | Ni (ppm) | Cu (ppm) | Zn (ppm) | As (ppm) | Se (ppm) | Mo (ppm) | Ru (ppm) | Rh (ppm) | Pd (ppm) | Ag (ppm) | Sn (ppm) | Sb (ppm) | Te (ppm) | Os (ppm) | Ir (ppm) | Pt (ppm) | Au (ppm) | Pb (ppm) | Bi (ppm) |
|---|---|---|---|---|---|---|---|---|---|---|---|---|---|---|---|---|---|---|---|---|---|---|---|
| Whole-rock values | LTV-7555 | BPU outside c.a. | 1.09 | 17 | 100 | 510 | 4570 | 19.6 | – | 25.1 | 0.0002 | 0.0004 | 0.009 | 10.3 | 2.0 | 11.9 | 0.5 | <0159 | 0.0001 | 0.008 | 0.012 | 78.8 | 0.8 |
| Recalculation 100%S | | | | 577 | 3394 | 17312 | 155128 | 666 | – | 853.4 | 0.005 | 0.015 | 0.314 | 349.6 | 67.9 | 403.9 | 18.3 | – | 0.0020 | 0.273 | 0.414 | 2673.5 | 26.5 |
| Whole-rock values | A4-15-01 | BPU c.a. | 6.53 | 28 | 140 | 200 | 620 | 10 | – | 37.0 | 0.0002 | 0.001 | 0.002 | 2.1 | <1 | 2.6 | – | 0.00020 | 0.0001 | 0.009 | 0.016 | 37.0 | 0.2 |
| Recalculation 100%S | | | | 159 | 793 | 1133 | 3513 | 56.7 | – | 209.6 | 0.001 | 0.004 | 0.014 | 11.9 | – | 14.7 | – | 0.00102 | 0.0003 | 0.053 | 0.089 | 209.6 | 1.1 |
| Whole-rock values | DC-69 | BPU xenolith | 5.90 | 157 | 670 | 930 | 190 | 65.2 | 1.9 | 28.4 | 0.008 | 0.001 | 0.036 | <0.5 | <1 | <0.2 | 0.5 | 0.00116 | 0.0008 | 0.013 | 0.282 | 0.2 | <0,1 |
| Recalculation 100%S | | | | 985 | 4202 | 5832 | 1192 | 408.9 | 12.0 | 178.3 | 0.047 | 0.009 | 0.226 | – | – | – | 3.0 | 0.00730 | 0.0051 | 0.082 | 1.768 | 0.9 | – |
| Whole-rock values | DC-70 | BPU xenolith | 4.45 | 26 | 130 | 140 | 320 | 15.2 | 1.6 | 28.0 | <5.0 | 0.0001 | 0.001 | 1.1 | <1 | 1.5 | <0,06 | <1.5 | 0.0001 | 0.010 | 0.003 | 24.5 | 0.3 |
| Recalculation 100%S | | | | 216 | 1081 | 1164 | 2661 | 126.0 | 13.3 | 232.8 | – | 0.001 | 0.007 | 9.1 | – | 12.7 | – | – | 0.0005 | 0.081 | 0.023 | 203.9 | 2.3 |
| Whole-rock values | DC-71 | BPU xenolith | 10.20 | 44 | 280 | 1060 | 480 | 9.0 | 0.1 | 11.0 | – | – | – | 0.5 | 4.0 | 0.5 | – | – | – | – | 0.228 | 19.0 | <0,1 |
| Recalculation 100%S | | | | 160 | 1016 | 3845 | 1741 | 32.6 | 0.5 | 39.9 | – | – | – | 1.8 | 14.5 | 1.8 | – | – | – | – | 0.827 | 68.9 | – |
| Whole-rock values | DC-80 | BPU xenolith | 1.15 | 25 | 123 | 646 | – | 24.6 | – | – | <2.5 | 0.0001 | 0.004 | – | – | 1.9 | – | <0.6 | 0.0001 | 0.003 | 0.650 | – | – |
| Recalculation 100%S | | | | 791 | 3957 | 20784 | – | 791.5 | – | – | – | 0.002 | 0.129 | – | – | 61.5 | – | – | 0.0026 | 0.084 | 20.913 | – | – |
| Whole-rock values | B1-384-26 | BPU xenolith | 3.74 | 152 | 900 | 3100 | 380 | 22.0 | 3.7 | 24.3 | 0.003 | 0.001 | 0.042 | 1.0 | <1 | 0.4 | 0.3 | <0.58 | 0.0002 | 0.009 | 0.016 | 19.0 | 0.4 |
| Recalculation 100%S | | | | 1504 | 8904 | 30668 | 3759 | 217.6 | 36.7 | 240.2 | 0.026 | 0.010 | 0.412 | 9.9 | – | 4.0 | 2.6 | – | 0.0030 | 0.092 | 0.160 | 188.1 | 4.0 |
| Whole-rock values | EC-07-A | BPU xenolith | 2.50 | 86 | 730 | 3965 | 160 | 22.0 | 2.4 | 2.8 | 0.001 | 0.001 | 0.058 | 1.4 | 3.0 | 3.0 | 0.3 | – | 0.0003 | 0.023 | 0.027 | 15.9 | 2.2 |
| Recalculation 100%S | | | | 1273 | 10804 | 58683 | 2368 | 325.6 | 35.5 | 40.7 | 0.016 | 0.019 | 0.864 | 20.7 | 44.4 | 44.4 | 4.1 | – | 0.0037 | 0.336 | 0.393 | 235.0 | 32.6 |
| Whole-rock values | B1-384-39 | Massive sulfide | 16.30 | 960 | 12500 | 11200 | 290 | 61.6 | 24.5 | 23.0 | 0.039 | 0.015 | 0.063 | 6.8 | <1 | <0.2 | 0.6 | 0.00852 | 0.0080 | 0.005 | 0.022 | 5.8 | 0.3 |
| Recalculation 100%S | | | | 2179 | 25423 | 28374 | 658 | 139.9 | 55.6 | 52.2 | 0.090 | 0.034 | 0.143 | 15.4 | – | – | 1.3 | 0.01934 | 0.0183 | 0.012 | 0.050 | 13.1 | 0.7 |
| Whole-rock values | B1-384-12 | Norite | 1.27 | 134 | 1570 | 6500 | 180 | 22.0 | 3.1 | <2 | 0.005 | 0.002 | 0.048 | 1.0 | 1.0 | 0.5 | – | 0.00060 | 0.0009 | 0.023 | 0.016 | 17.0 | <0,1 |
| Recalculation 100%S | | | | 3904 | 45740 | 189370 | 5244 | 640.9 | 89.7 | – | 0.136 | 0.060 | 1.395 | 29.1 | 29.1 | – | – | 0.01806 | 0.0274 | 0.660 | 0.452 | 495 | – |
| Whole-rock values | B1-384-13 | Norite | 1.72 | 108 | 786 | 2164 | 51 | 8.2 | 1.9 | – | 0.004 | 0.001 | 0.027 | 2.3 | – | 1.2 | – | <0.42 | 0.0003 | 0.010 | 0.013 | – | – |
| Recalculation 100%S | | | | 2329 | 16908 | 46551 | 1104 | 176.4 | 40.2 | – | 0.095 | 0.019 | 0.583 | 48.8 | – | 25.8 | – | – | 0.0069 | 0.221 | 0.275 | – | – |
| Whole-rock values | B1-384-16 | Norite | 7.17 | 81 | 470 | 1830 | 670 | 29.0 | 3.0 | <2 | 0.005 | 0.004 | 0.037 | 0.5 | <1 | <0.2 | – | 0.0007 | 0.0021 | 0.009 | 0.033 | 8.0 | 0.2 |
| Recalculation 100%S | | | | 418 | 2425 | 9444 | 3457 | 149.7 | 15.4 | – | 0.026 | 0.022 | 0.190 | 2.6 | – | – | – | 0.0040 | 0.0108 | 0.048 | 0.172 | 41.3 | 1.0 |
| Whole-rock values | EC-07-B | Norite | 0.05 | 26 | 60 | 300 | 60 | – | 0.2 | <2 | – | – | 0.001 | 0.6 | <1 | 0.4 | – | – | – | 0.001 | – | – | 0.2 |
| Recalculation 100%S | | | | n.d. | n.d. | n.d. | n.d. | n.d. | n.d. | n.d. | n.d. | n.d. | n.d. | n.d. | n.d. | n.d. | n.d. | n.d. | n.d. | n.d. | n.d. | n.d. | n.d. |
| Whole-rock values | B1-384-04b | Gabbronorite | 0.03 | 79 | 410 | 920 | 200 | 11.0 | 0.04 | 3.0 | 0.003 | 0.002 | 0.071 | 0.6 | 2.0 | <0.2 | – | 0.00030 | 0.0009 | 0.027 | 0.006 | 14.0 | <0,1 |
| Recalculation 100%S | | | | n.d. | n.d. | n.d. | n.d. | n.d. | n.d. | n.d. | n.d. | n.d. | n.d. | n.d. | n.d. | n.d. | n.d. | n.d. | n.d. | n.d. | n.d. | n.d. | n.d. |
| Whole-rock values | B1-384-05 | Gabbronorite | 1.77 | 129 | 650 | 760 | 150 | <5 | 0.4 | <2 | 0.018 | 0.019 | 0.427 | <0.5 | <1 | <0.2 | <0.06 | 0.00300 | 0.0041 | 0.109 | 0.192 | <5 | <0,1 |
| Recalculation 100%S | | | | 2697 | 13588 | 15887 | 3136 | – | 8.8 | – | 0.375 | 0.404 | 8.924 | – | – | – | – | 0.05560 | 0.0851 | 2.286 | 4.016 | – | – |
| Whole-rock values | B1-384-08 | Gabbronorite | 1.80 | 116 | 1804 | 7718 | 89 | <0.73 | 10.9 | – | 0.023 | 0.039 | 1.393 | 3.9 | – | 0.4 | 1.4 | 0.002 | 0.0100 | 0.420 | 0.170 | – | – |
| Recalculation 100%S | | | | 2383 | 37082 | 158648 | 1819 | – | 224.3 | – | 0.463 | 0.807 | 28.643 | 79.3 | – | 7.4 | 27.9 | 0.04100 | 0.2100 | 8.680 | 3.490 | – | – |
| Whole-rock values | B1-384-21 | Gabbronorite | 0.29 | 87 | 390 | 2070 | 150 | <5 | 0.7 | <2 | <2.1 | 0.0003 | 0.016 | 1.7 | 2.0 | <0.2 | – | <0.46 | 0.0002 | 0.005 | 0.008 | 7.0 | <0,1 |
| Recalculation 100%S | | | | 11100 | 49759 | 264103 | 19138 | – | 91.9 | – | – | 0.042 | 2.100 | 216.9 | 255.2 | – | – | – | 0.0217 | 0.646 | 0.957 | 893 | – |

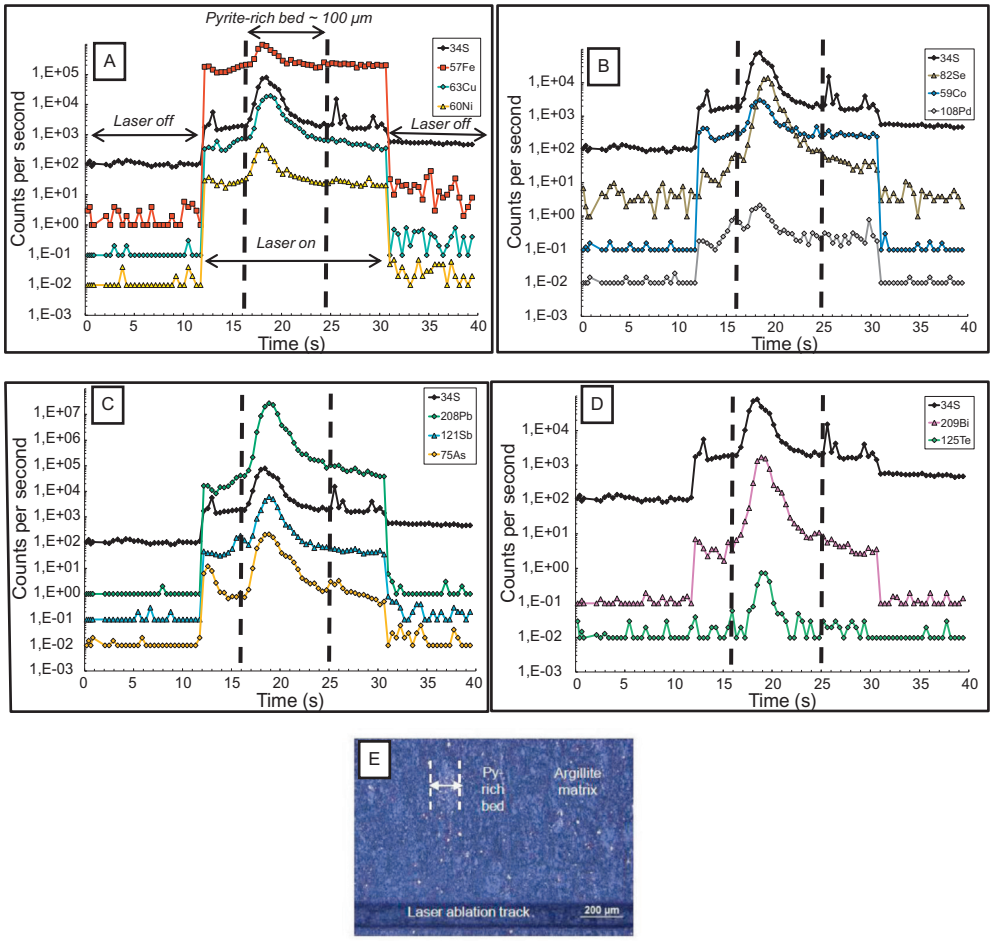


**Fig. 7.** LA-ICP-MS time-signal diagrams for a pyrite-rich bed in Bedded Pyrrhotite Unit (BPU) from outside the contact aureole (see photomicrograph E). Signals of TABS and trace metals are obtained after laser ablation (line scans) across pyrite beds in a Bedded Pyrrhotite Unit (BPU) sample from outside the contact aureole with beam size of 75 µm, power of 25 Hz and speed of 10 µm/s. The counts per second for some elements are multiplied, or divided, by 10–100 to improve the clarity. Abbreviation: Py = Pyrite.

the sulfide liquid during the sulfide segregation process from a mafic magma, but the TABS do not partition into the mss (monosulfide solid solution) and iss (intermediate solid solution) that crystallize from the sulfide liquid and hence they concentrate into the fractionated sulfide liquid along with Pt and Pd.

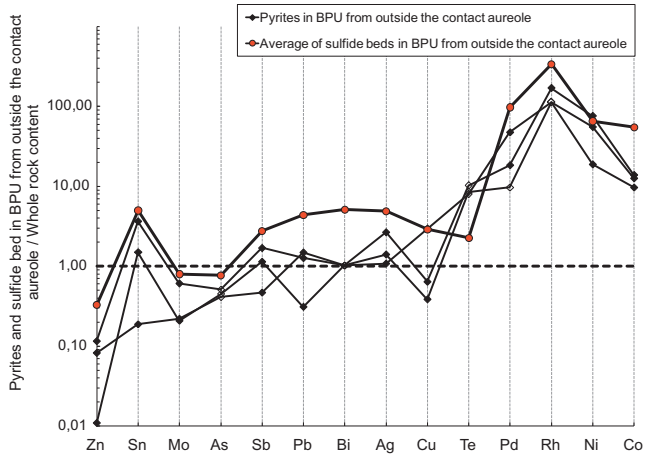


**Fig. 8.** Diagram of trace metal and TABS contents of sedimentary pyrites of the Bedded Pyrrhotite Unit (BPU) from outside the contact aureole normalized to whole-rock concentrations. Dotted lines correspond to 1:1 ratio in the diagram. Blank symbols are employed for values which are below the detection limits. Abbreviation: BPU = Bedded Pyrrhotite Unit.

Some PGM and other TABS minerals crystallize from the fractionated sulfide liquid and consequently, are commonly found in association with chalcopyrite and cubanite. These minerals can also form subsolidus phases during exsolution of mss and iss to form pyrrhotite, pentlandite, chalcopyrite and cubanite. At this stage TABS and PGE may be pushed to the grain boundaries, or into dislocations, and they form PGM and TABS minerals. The laser maps of As, Sb, Sn, Pb and Bi distributions in the Bedded Pyrrhotite Unit xenoliths and the mafic rocks of the Duluth Complex show that these elements are concentrated within the area outlined by clusters of base metal sulfide minerals and close to Cu-rich minerals, but their distribution is irregular suggesting that they are present as inclusions within the sulfides. This interpretation is supported by the observation of Sn, Pb and Bi platinum group minerals associated with chalcopyrite (Fig. 4 and Table 2). In our study we did not observe Sb and As platinum group minerals, but previous studies report the presence of As- and Sb- bearing minerals maucherite, niccolite and gersdorffite with Cu-rich sulfides in the mafic rocks of the basal magmatic units (McSwiggen, 1999; Thériault et al., 1997; Severson and Hauck, 2003; Table 6a; Cervin, 2011).

In addition to sulfides and PGM the laser maps indicate that silicate phases also contain Sn and Pb in the rocks of the Bedded Pyrrhotite Unit from the contact aureole, the Bedded Pyrrhotite Unit xenoliths and the mafic rocks of the Duluth Complex. Plagioclase and orthopyroxene host respectively Pb and Sn (Figs. 10 to 12; Johnson et al., 2013) in the Duluth Complex.

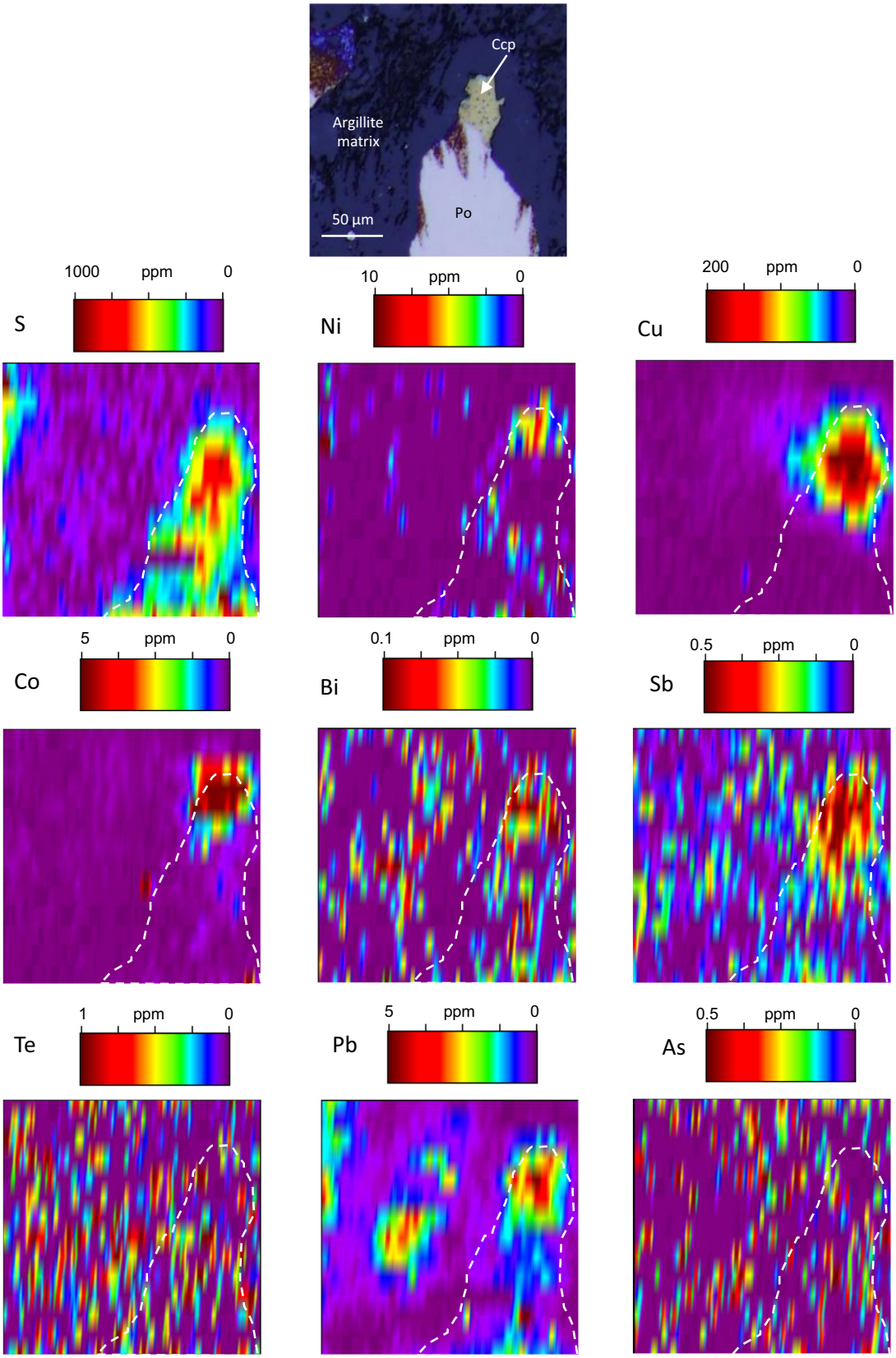


**Fig. 9.** LA-ICP-MS maps of sulfide bed in Bedded Pyrrhotite Unit (BPU) from outside the contact aureole. Maps are obtained after ablation of a BPU sample from outside the contact aureole with beam size of 5 µm, frequency of 20 Hz and fluence of 10 J/cm$^2$.

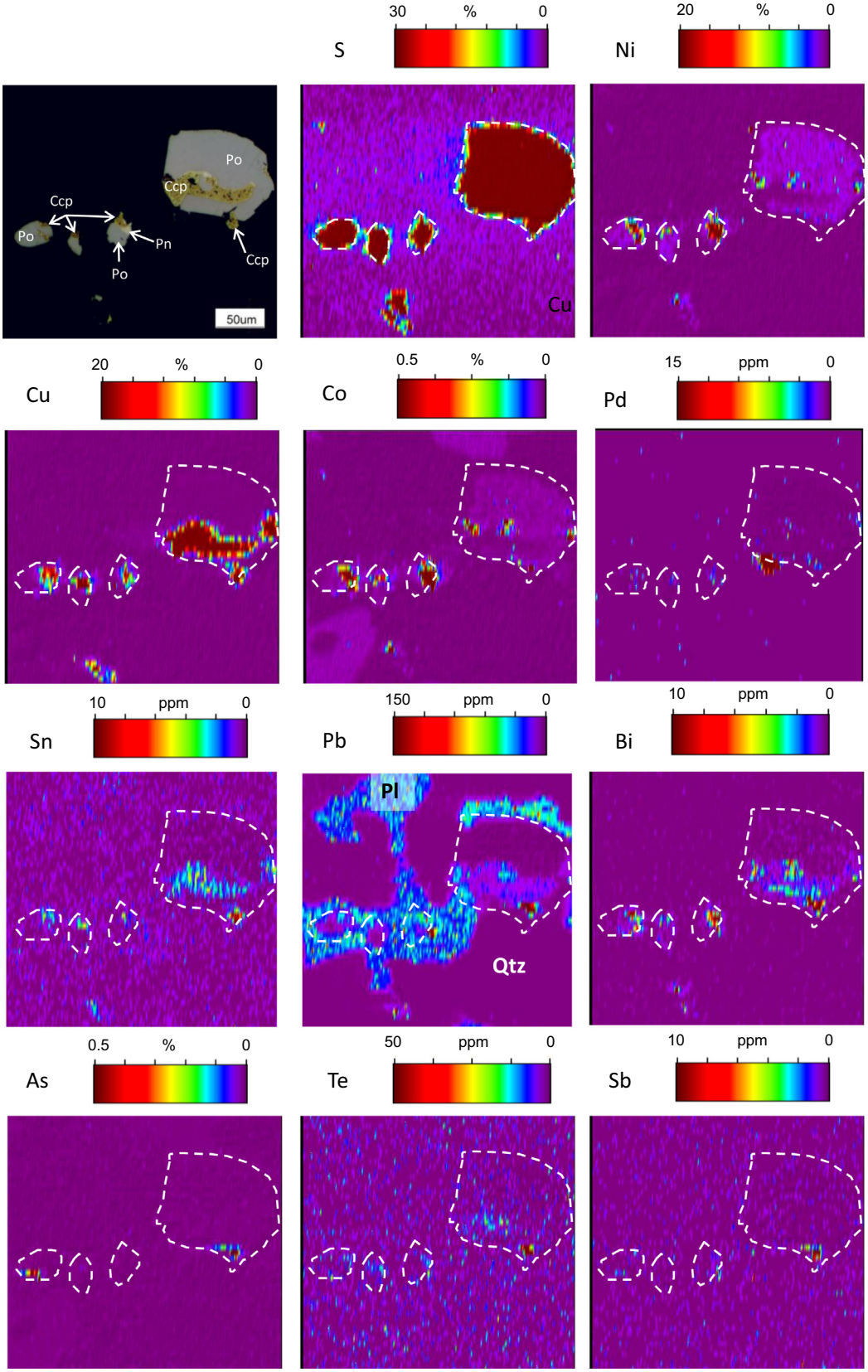


**Fig. 10.** LA-ICP-MS maps of droplets of sulfide trapped in the anatectic melt in a xenolith of Bedded Pyrrhotite Unit (BPU). Maps are obtained after ablation of a BPU xenolith with beam size of 5 μm, frequency of 20 Hz and fluence of 10 J/cm$^2$. Abbreviation: Pl = plagioclase, Qtz = quartz.

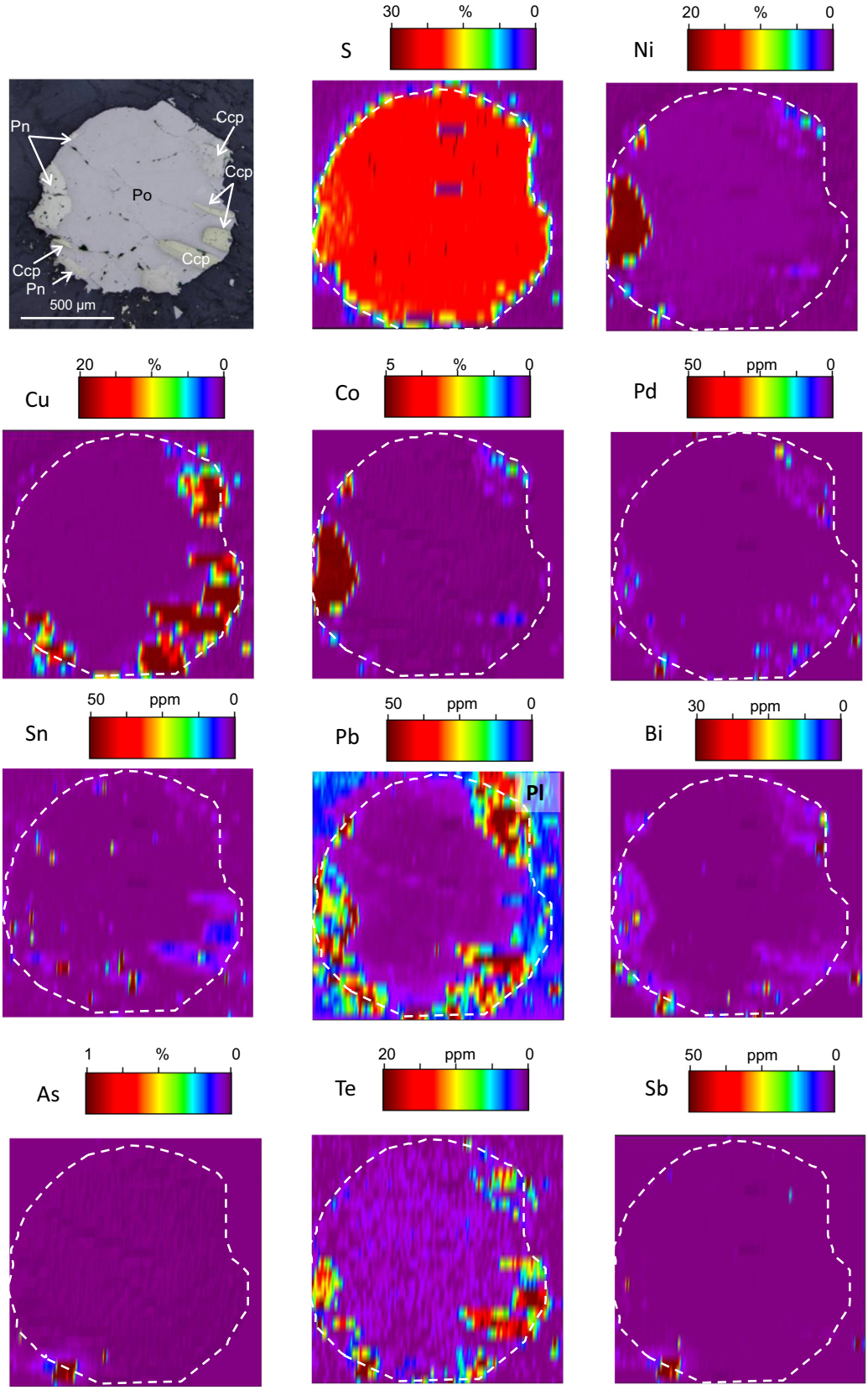


**Fig. 11.** LA-ICP-MS maps of droplets of sulfide trapped in the mafic magma surrounding xenoliths of Bedded Pyrrhotite Unit (BPU), i.e. norite. Maps are obtained after ablation of norite with beam size of 44 µm, frequency of 15 Hz and fluence of 3 J/cm$^2$.

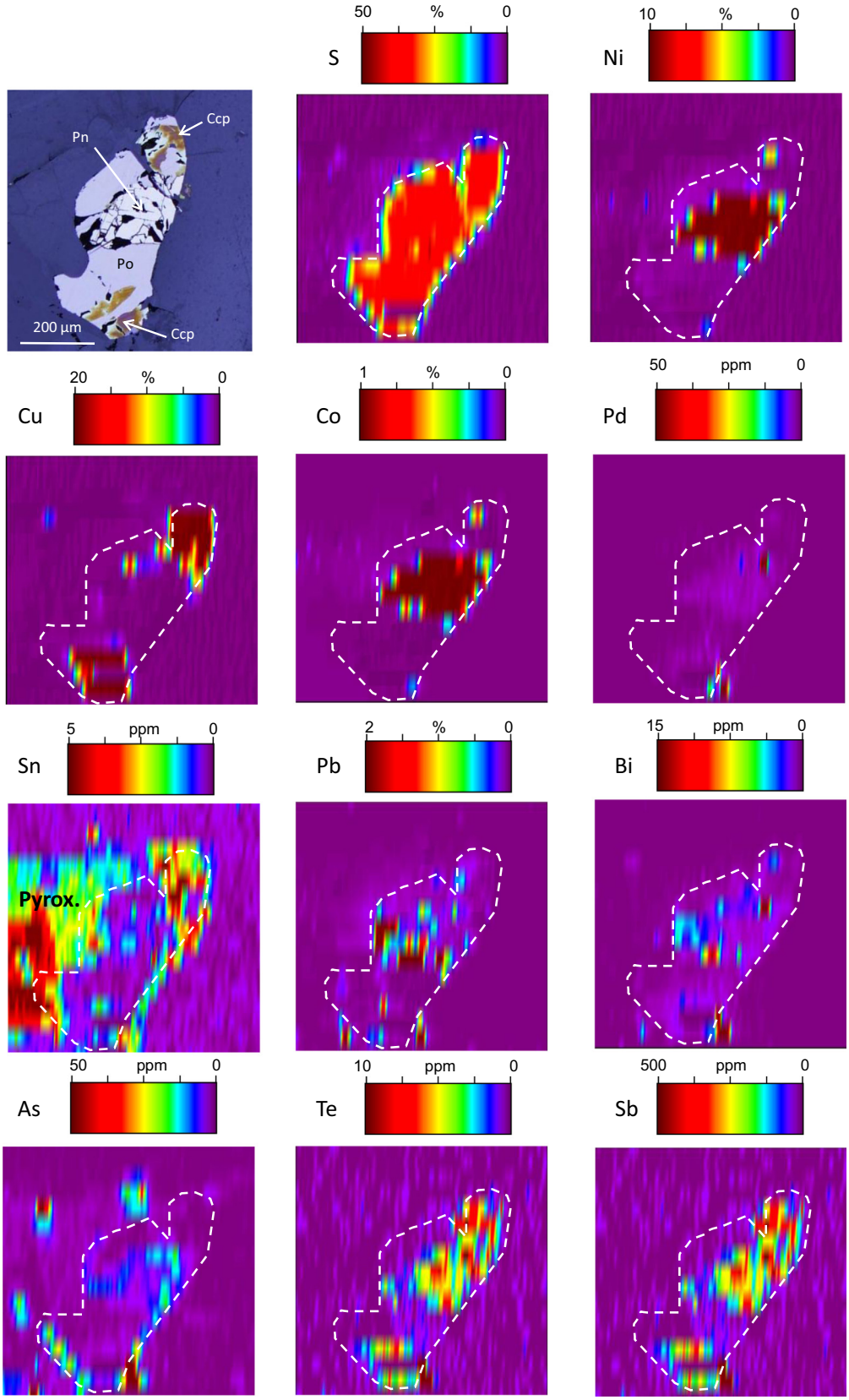


**Fig. 12.** LA-ICP-MS maps of sulfide droplets trapped in gabbronorite. Maps are obtained after ablation of gabbronorite with beam size of 44 µm, frequency of 15 Hz and fluence of 3 J/cm$^2$.

*5.1.2. Least metamorphosed Bedded Pyrrhotite Unit from outside the contact aureole*

In contrast to the distribution of TABS in the contact aureole and within the intrusion the least metamorphosed samples of the Bedded Pyrrhotite Unit from outside the contact aureole most of the TABS are concentrated in galena, pyrite and pyrrhotite.

Pyrites in these samples have similar TABS contents to the compilation of analyzes of sedimentary pyrites in Gregory et al. (2015) and are enriched in TABS in comparison with magmatic pyrite from the literature (Dare et al., 2011; Piña et al., 2013; Duran et al., 2015) (Fig. 13). Syngenetic and diagenetic sedimentary pyrites may have been enriched in TABS during their formation in sedimentary basins (Morse, 1999; Morse and Luther, 1999; Chappaz et al., 2014), i.e., after deposition of sulfidic sediments enriched in organic matter (now observed as black shales) in sedimentary basins. In addition, pyrites of the least metamorphosed Bedded Pyrrhotite Unit from outside the contact aureole have lower contents of Co and platinum-group elements than magmatic pyrites from the literature (Fig. 13); the level of most of the platinum-group elements from the Bedded Pyrrhotite Unit pyrites are below the detection limits.

Mass balance estimations for the least metamorphosed samples of the Bedded Pyrrhotite Unit from outside the contact aureole are done by comparing TABS contents in each phase, i.e., data obtained by LA-ICP-MS, with whole rock data and show that the TABS content of the pyrites is similar to the whole rock values (Fig. 8). However, the rock contains <2% pyrite thus the TABS must be present in other phase as well. The sulfide beds as whole are enriched in TABS by a factor of ~3, but as the rock contains <3% sulfide minerals TABS must also be present in other phase. Galena and Sb-rich phases were observed in the heavy mineral bed and galena contains significant amounts of Ag, Cd, Sn. Sb, Te and Bi and thus may be the host of some of the elements. Colloidal phases (consisting of organic compounds) absorb semimetals during sedimentary basin formation (Buffle and Leppard, 1995; Gustafsson and Gschwend, 1997; Gustafsson et al., 2000) and possibly the missing chalcophile elements are present in this form.

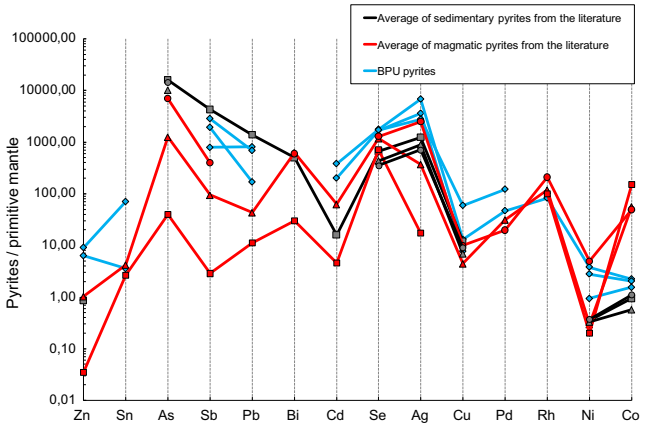


**Fig. 13.** Mantle-normalized plot of averages of TABS content and trace metals contents of the pyrites in the Bedded Pyrrhotite Unit (BPU) and from the literature. Averages of magmatic (Dare et al., 2011; Piña et al., 2013; Duran et al., 2015) and sedimentary pyrites (Gregory et al., 2015) are shown for reference. Symbols for diagram (A): Grey triangle = Average of Paleoproterozoic pyrites in black shales (n = 105); Grey circle = Average of small euhedral pyrites in black shales (n = 92); Grey square = Compilation of pyrites in black shales; Red triangle = Average of pyrites in Lac des Iles deposit (n = 57); Red circle = Average of pyrites in Aguablanca deposit (n = 32); Red square = Average of pyrites in Mc Creedy deposit (n = 23). Abbreviation: BPU = Bedded Pyrrhotite Unit.

*5.2. Implications for the deposits formation*

The TABS are important elements for PGM formation in numerous Ni-Cu-PGE deposits. Based on whole rock analyzes, a source of TABS in the sulfide deposits of the Partridge River Intrusion of the Duluth Complex is black shales of the Bedded Pyrrhotite Unit (Samalens et al., 2017). Xenoliths of the Bedded Pyrrhotite Unit were trapped in the mafic magma during the intrusion emplacement and have undergone partial melting within. Our LA-ICP-MS study shows that sulfides in the Bedded Pyrrhotite Unit xenoliths and sulfide droplets in the gabbronorites and norites concentrate most of the TABS. In addition, LA-ICP-MS maps of sulfide droplets trapped inside the anatectic melt in the xenoliths of Bedded Pyrrhotite Unit show that these sulfide droplets carry TABS. The results of the LA-ICP-MS study support the model proposed by Samalens et al. (2017) of TABS contamination of the mafic magma after transfer by advection of TABS-rich sulfide droplets from the xenoliths of the Bedded Pyrrhotite Unit to the mafic magma.

However, although chalcopyrite, pentlandite, pyrite and pyrrhotite contain some TABS, our study shows that other phases galena, PGM and silicate phases host a part of the TABS budget.

## 6. Conclusions

Our LA-ICP-MS study shows that most of the TABS are associated with Cu-rich sulfides and pentlandite in the rocks of the Bedded Pyrrhotite Unit from the contact aureole, the xenoliths of the Bedded Pyrrhotite Unit and the mafic rocks of the Duluth Complex. However, these elements are also partitioned into platinum-group minerals and silicate phases (i.e. Pb in plagioclase and Sn in orthopyroxene) in these rocks. In contrast, in the least metamorphosed black shales from outside the contact aureole, TABS are partitioned among pyrite pyrrhotite, galena and Sb-rich phases. In addition, organic compounds may have concentrated some chalcophile elements.

The TABS contamination of the magma by black shales plays an important role in forming the deposit formation because TABS are important in the PGM formation. The distribution of TABS among phases at the Duluth Complex support previous model of TABS contamination of mafic magma by assimilation of xenoliths of the Bedded Pyrrhotite Unit, i.e., transfer by advection of TABS-rich sulfide droplets from the xenoliths to the magma. In addition to the Duluth Complex, formation of numerous Ni-Cu-PGE deposits that contain PGM may require TABS contamination of the magma by back shales.

## Acknowledgments

This work was funded by a Canadian Natural Science and Engineering Research Council Discovery Grant to SJB (17313) and a Canada Research Chair program grant to SJB (215503). We thank Mark Severson for providing some samples of the Bedded Pyrrhotite Unit from the contact aureole. Sadia Medhi, Dany Savard and Marko Kudrna Prašek from LabMaTer are thanked to help in carrying out analyzes. We would like to thank Dr. Valentina Taranovic and an anonymous reviewer for helping us improve the clarity of our arguments. Professor Franco Pirajno and Prof. Marco Fiorentini are also thanked for their editorial handling.

## Appendix A. Supplementary data

Supplementary data associated with this article can be found, in the online version, at http://dx.doi.org/10.1016/j.oregeorev.2017.06.007.

## References


Andrews, D., Ripley, E.M., 1989. Mass transfer and sulfur fixation in the contact aureole of the Duluth Complex, Dunka Road Cu-Ni deposit, Minnesota. Can. Mineral. 27, 293–310.

Barnes, S.-J., Lightfoot, P.C., 2005. Formation of magmatic nickel-sulfide ore deposits and processes affecting their copper and platinum-group elements contents. Econ. Geol., 179–213 100th Anniversary.

Barnes, S.-J., Ripley, E.M., 2016. Highly siderophile and strongly chalcophile elements in magmatic ore deposits. Rev. Mineral. Geochem. 81, 725–774.

Barnes, S.-J., Makovicky, E., Makovicky, M., Rose-Hansen, J., Karup-Moller, S., 1997. Partition coefficients for Ni, Cu, Pd, Pt, Rh, and Ir between monosulfide solid solution and sulfide liquid and the formation of compositionally zoned Ni – Cu sulfide bodies by fractional crystallization of sulfide liquid. Can. J. Earth Sci. 34, 366–374.

Bédard, L.P., Savard, D., Barnes, S.-J., 2008. Total sulfur concentration in geological reference materials by elemental infrared analyzer. Geostand. Geoanal. Res. 32, 203–208.

Benkó, Z., Mogessie, A., Molnár, F., Krenn, K., Poulson, S.R., Hauck, S.A., Severson, M. J., Arehart, G.B., 2015a. Hydrothermal alteration and Cu–Ni–PGE mobilization in the charnockitic rocks of the footwall of the South Kawishiwi intrusion, Duluth Complex, USA. Ore Geol. Rev. 67, 170–188.

Benkó, Z., Mogessie, A., Molnár, F., Severson, M.J., Hauck, S.A., Raič, S., 2015b. Partial Melting Processes and Cu-Ni-PGE Mineralization in the Footwall of the South Kawishiwi Intrusion at the Spruce Road Deposit, Duluth Complex, Minnesota. Econ. Geol. 110, 1269–1293.

Bonnichsen, W., 1972. Sulfide minerals in the Duluth Complex. In: Sims, P.K., Morey, G.W. (Eds.), Geology of Minnesota: A Centennial Volume: Minn. Geol. Survey, pp. 388–393.

Buffle, J., Leppard, G.G., 1995. Characterization of aquatic colloids and macromolecules. 1. Structure and behavior of colloidal material. Environ. Sci. Technol. 29, 2169–2175.

Cervin, D.O., 2011. Characterization of precious metal mineral occurrences in the NorthMet deposit of the Partridge River Intrusion, Duluth complex, Minnesota, USA: Unpublished. M.Sc. thesis, University of Minnesota, pp. 155.

Chappaz, A., Lyons, T.W., Gregory, D.D., Reinhard, C.T., Gill, B.C., Li, C., Large, R.R., 2014. Does pyrite act as an important host for molybdenum in modern and ancient euxinic sediments? Geochim. Cosmochim. Acta 126, 112–122.

Chen, L.-M., Song, X.-Y., Danyushevsky, L.V., Wang, Y.-S., Tian, Y.-L., Xiao, J.-F., 2015. A laser ablation ICP-MS study of platinum-group and chalcophile elements in base metal sulfide minerals of the Jinchuan Ni–Cu sulfide deposit, NW China. Ore Geol. Rev. 65, 955–967.

Dare, S., Barnes, S.-J., Prichard, H., 2010. The distribution of platinum group elements (PGE) and other chalcophile elements among sulfides from the Creighton Ni–Cu–PGE sulfide deposit, Sudbury, Canada, and the origin of palladium in pentlandite. Miner. Deposita 45, 765–793.

Dare, S., Barnes, S.-J., Prichard, H., Fisher, P., 2011. Chalcophile and platinum-group element (PGE) concentrations in the sulfide minerals from the McCreedy East deposit, Sudbury, Canada, and the origin of PGE in pyrite. Miner. Deposita 46, 381–407.

Duran, C.J., Barnes, S.-J., Corkery, J.T., 2015. Chalcophile and platinum-group element distribution in pyrites from the sulfide-rich pods of the Lac des Iles Pd deposits, Western Ontario, Canada: implications for post-cumulus re-equilibration of the ore and the use of pyrite compositions in exploration. J. Geochem. Explor. 158, 223–242.

Duran, C.J., Barnes, S.-J., Corkery, J.T., 2016. Trace element distribution in primary sulfides and Fe–Ti oxides from the sulfide-rich pods of the Lac des Iles Pd deposits, Western Ontario, Canada: constraints on processes controlling the composition of the ore and the use of pentlandite compositions in exploration. J. Geochem. Explor. 166, 45–63.

Gál, B., Molnár, F., Guzmics, T., Mogessie, A., Szabó, C., Peterson, D.M., 2013. Segregation of magmatic fluids and their potential in the mobilization of platinum-group elements in the South Kawishiwi Intrusion, Duluth Complex, Minnesota - Evidence from petrography, apatite geochemistry and coexisting fluid and melt inclusions. Ore Geol. Rev. 54, 59–80.

Godel, B., Barnes, S.-J., Maier, W.D., 2007. Platinum-group elements in sulphide minerals, platinum-group minerals, and whole-rocks of the Merensky Reef (Bushveld Complex, South Africa): implications for the formation of the reef. J. Petrol. 48, 1569–1604.

Gregory, D.D., Large, R.R., Halpin, J.A., Baturina, E.L., Lyons, T.W., Wu, S., Danyushevsky, L., Sack, P.J., Chappaz, A., Maslennikov, V.V., Bull, S.W., 2015. Trace element content of sedimentary pyrite in black shales. Econ. Geol. 110, 1389–1410.

Gustafsson, Ö., Gschwend, P.M., 1997. Aquatic colloids: concepts, definitions, and current challenges. Limnol. Oceanogr. 42, 519–528.

Gustafsson, Ö., Widerlund, A., Andersson, P.S., Ingri, J., Roos, P., Ledin, A., 2000. Colloid dynamics and transport of major elements through a boreal river-brackish bay mixing zone. Mar. Chem. 71, 1–21.

Hauck, S.A., Severson, M.J., Zanko, L., Barnes, S.-J., Morton, P., Alminas, H., Foord, E.E., Dahlberg, E.H., 1997. An overview of the geology and oxide, sulfide, and platinum-group element mineralization along the western and northern contacts of the Duluth Complex. Geol. Soc. Am. Special paper 312, 137–185.

Henrique-Pinto, R., Barnes, S.-J., Savard, D., Mehdi, S., 2017. Quantification of metals and semimetals in carbon-rich rocks: a new sequential protocol including extraction from humic substances. Geostand. Geoanal. Res. 41, 41–62.

Holwell, D.A., McDonald, I., 2007. Distribution of platinum-group elements in the Platreef at Overysel, northern Bushveld Complex: a combined PGM and LA-ICP-MS study. Contrib. Mineral. Petrol. 154, 171–190.

Hutchinson, D., McDonald, I., 2008. Laser ablation ICP-MS study of platinum-group elements in sulphides from the Platreef at Turfspruit, northern limb of the Bushveld Complex, South Africa. Miner. Deposita 43, 695–711.

Johnson, E.R., Kamenetsky, V.S., McPhie, J., 2013. The Behavior of Metals (Pb, Zn, As, Mo, Cu) during crystallization and degassing of rhyolites from the Okataina Volcanic Center, Taupo Volcanic Zone, New Zealand. J. Petrol. 54, 1641–1659.

Labotka, T.C., Papike, J.J., Vaniman, D.T., 1981. Petrology of contact metamorphosed argillite from the Rove Formation, Gunflint Trail, Minnesota. Am. Mineral. 66, 70–86.

Lesher, C.M., Burnham, O.M., 2001. Multicomponent elemental and isotopic mixing in Ni–Cu–(PGE) ores at Kambalda, Western Australia. Can. Mineral. 39, 421–446.

Lucente, M.E., Morey, G.B., 1983. Stratigraphy and sedimentology of the Lower Proterozoic Virginia Formation, northern Minnesota. Minnesota Geological Survey, Report of Investigations RI-28, pp. 28.

Mainwaring, P.R., Naldrett, A., 1977. Country-rock assimilation and the genesis of Cu-Ni sulfides in the water hen intrusion, duluth complex, Minnesota. Econ. Geol. 72, 1269–1284.

McSwiggen, P.L., 1999. Platinum-palladium group minerals, gold, silver, and cobalt in the Minnamax copper-nickel sulfide deposit, Duluth Complex, northeastern Minnesota. Minnesota Geological Survey, Report of Investigations RI-54, pp. 29.

Miller, J.D., Jr., Severson, M.J., 2002, Geology of the Duluth Complex, In: Miller, J.D., Jr., Green, J.C., Severson, M.J., Chandler, V.W., Hauck, S.A., Peterson, D.M., and Wahl, T.E., (Eds.), Geology and mineral potential of the Duluth Complex and related rocks of northeastern Minnesota: Minnesota Geological Survey, Report of Investigations RI-58, pp. 106–143.

Morse, J.W., 1999. Sulfides in sandy sediments: new insights on the reactions responsible for sedimentary pyrite formation. Aquat. Geochem. 5, 75–85.

Morse, J.W., Luther, G.W., 1999. Chemical influences on trace metal-sulfide interactions in anoxic sediments. Geochim. Cosmochim. Acta 63, 3373–3378.

Ojakangas, R.W., Morey, G.B., Green, J.C., 2001. The Mesoproterozoic midcontinent rift system, Lake Superior Region, USA. Sediment. Geol. 141–142, 421–442.

Osbahr, I., Klemd, R., Oberthür, T., Brätz, H., Schouwstra, R., 2013. Platinum-group element distribution in base-metal sulfides of the Merensky Reef from the eastern and western Bushveld Complex, South Africa. Miner. Deposita 48, 211–232.

Piña, R., Gervilla, F., Barnes, S.-J., Ortega, L., Lunar, R., 2012. Distribution of platinum-group and chalcophile elements in the Aguablanca Ni–Cu sulfide deposit (SW Spain): evidence from a LA-ICP-MS study. Chem. Geol. 302, 61–75.

Piña, R., Gervilla, F., Barnes, S.-J., Ortega, L., Lunar, R., 2013. Platinum-group elements-bearing pyrite from the Aguablanca Ni-Cu sulphide deposit (SW Spain): a LA-ICP-MS study. Eur. J. Mineral. 25, 241–252.

Queffurus, M., Barnes, S.-J., 2014. Selenium and sulfur concentrations in country rocks from the Duluth Complex, Minnesota, USA: implications for formation of the Cu-Ni-PGE sulfides. Econ. Geol. 109, 785–794.

Raič, S., Mogessie, A., Benkó, Z., Molnár, F., Hauck, S., Severson, M., 2015. Arsenic-rich Cu-Ni-PGE mineralization in Wetlegs, Duluth Complex, St. Louis County, Minnesota, USA. Can. Mineral. 53, 1–28.

Ripley, E.M., 1981. Sulfur isotopic studies of the Dunka road Cu-Ni deposit, Duluth Complex, Minnesota. Econ. Geol. 76, 610–620.

Ripley, E.M., 2014. Ni-Cu-PGE Mineralization in the Partridge River, South Kawishiwi, and Eagle Intrusions: a review of contrasting styles of sulfide-rich occurrences in the Midcontinent Rift System. Econ. Geol. 109, 309–324.

Ripley, E.M., Alawi, J.A., 1988. Petrogenesis of pelitic xenoliths at the Babbitt Cu-Ni deposit, Duluth Complex, Minnesota, U.S.A. Lithos 21, 143–159.

Ripley, E.M., Li, C., 2013. Sulfide saturation in mafic magmas: is external sulfur required for magmatic Ni-Cu-(PGE) ore genesis? Econ. Geol. 108, 45–58.

Ripley, E.M., Taib, N.I., Chusi, L., Moore, C.H., 2007. Chemical and mineralogical heterogeneity in the basal zone of the Partridge River Intrusion: implications for the origin of Cu–Ni sulfide mineralization in the Duluth Complex, Midcontinent Rift System. Contrib. Mineral. Petrol. 154, 35–54.

Robertson, J., Ripley, E.M., Barnes, S.J., Li, C., 2015. Sulfur liberation from country rocks and incorporation in mafic magmas. Econ. Geol. 110, 1111–1123.

Samalens, N., Barnes, S.-J., Sawyer, E.W., 2017. The role of black shales as a source of sulfur and semimetals in magmatic nickel-copper deposits: example from the Partridge River Intrusion, Duluth Complex, Minnesota, USA. Ore Geol Rev. 81, 173–187.

Savard, D., Bédard, L.P., Barnes, S.J., 2006. TCF selenium preconcentration in geological materials for determination at sub-μgg− 1 with INAA (Se/TCF-INAA). Talanta 70, 566–571.

Savard, D., Barnes, S.-J., Meisel, T., 2010. Comparison between nickel-sulfur fire assay Te Co-precipitation and isotope dilution with high-pressure Asher acid digestion for the determination of platinum-group elements, rhenium and gold. Geostand. Geoanal. Res. 34, 281–291.

Sawyer, E.W., 2014. The inception and growth of leucosomes: microstructure at the start of melt segregation in migmatites. J. Metamorph. Geol. 7, 695–712.

Severson, M.J., Hauck, S.A., 1997. Igneous stratigraphy and mineralization in the basal portion of the Partridge River Intrusion, Duluth Complex, Allen Quadrangle, Minnesota: Duluth, Minnesota. University of Minnesota, Natural Resources Research Institute, Technical Report, NRRI/TR-97/19, p.p. 102.

Severson, M.J., Hauck, S.A., 2003. Platinum group elements (PGEs) and platinum group minerals (PGMs) in the Duluth Complex: Duluth, Minnesota. University

of Minnesota, Natural Resources Research Institute, Technical Report, NRRI/TR-2003/37, pp. 312.
Severson, M.J., Hauck, S.A., 2008. Finish logging of Duluth Complex Drill Core (and a reinterpretation of the geology at the Mesaba (Babbitt) deposit): Duluth. University of Minnesota, Natural Resources Research Institute, Technical Report, NRRI/TR-2008/17, pp. 68.
Thériault, R.D., Barnes, S.-J., 1998. Compositional variations in Cu-Ni-PGE sulfides of the Dunka road deposit, Duluth Complex, Minnesota: the importance of combined assimilation and magmatic processes. Can. Mineral. 36, 869–886.
Thériault, R.D., Barnes, S.-J., Severson, M.J., 1997. The influence of country-rock assimilation and silicate to sulfide ratios (R factor) on the genesis of the Dunka Road Cu – Ni – platinum-group element deposit, Duluth Complex, Minnesota. Can. J. Earth Sci. 34, 375–389.
Thériault, R.D., Barnes, S.-J., Severson, M.J., 2000. Origin of Cu-Ni-PGE Sulfide Mineralization in the Partridge River Intrusion, Duluth Complex, Minnesota. Econ. Geol.
Tracy, R.J., Frost, B.R., 1991. Phase equilibria and thermobarometry of calcareous, ultramafic and mafic rocks, and iron formations. Rev. Mineral. Geochem. 26, 207–289.
Zanko, L.M., Severson, M.J., Ripley, E.M., 1994. Geology and mineralization of the Serpentine copper-nickel deposit, Duluth Complex, Minnesota. Duluth. University of Minnesota, Natural Resources Research Institute, Technical Report, NRRI/TR-93/52, pp. 90.